

## Charge cross-over at the $U(1)$ -Higgs phase transition

Filipe Freire <sup>a,b\*</sup> and Daniel F. Litim <sup>c†</sup>

<sup>a</sup>*Department of Mathematical Physics, N.U.I. Maynooth, Ireland.*

<sup>b</sup>*School of Theoretical Physics, Dublin Institute for Advanced Studies  
10 Burlington Road, Dublin 4, Ireland.*

<sup>c</sup>*Institut für Theoretische Physik, Philosophenweg 16  
D-69120 Heidelberg, Germany.*

### Abstract

The type-I region of phase transitions at finite temperature of the  $U(1)$ -Higgs theory in 3+1 dimensions is investigated in detail using a Wilsonian renormalisation group. We consider in particular the quantitative effects induced through the cross-over of the scale-dependent Abelian charge from the Gaussian to a non-trivial Abelian fixed point. As a result, the strength of the first-order phase transition is weakened. Analytical solutions to approximate flow equations are obtained, and all characteristics of the phase transition are discussed and compared to the results obtained from perturbation theory. In addition, we present a detailed quantitative study regarding the dependence of the physical observables on the coarse-graining scheme. This results in error-bars for the regularisation scheme (RS) dependence. We find quantitative evidence for an intimate link between the RS dependence and truncations of flow equations.

PACS numbers: 11.10.Wx 11.10.Hi 11.15.Tk 05.70.Fh

---

\*freire@thphys.may.ie

†Daniel.Litim@cern.ch

Present address: Theory Division, CERN, CH – 1211 Geneva 23.

## I. INTRODUCTION

The phase transition of the  $U(1)$ -Higgs theory in 3+1 dimensions at finite temperature provides an important model for cosmological phase transitions. In the high temperature limit, it reduces to the purely  $3d$  Abelian Higgs model describing the superconducting phase transition [1], or certain nematic to smectic-A phase transitions in liquid crystals [2]. The phase transition in this model is governed by the infra-red region of its spectrum of fluctuations. The nature of the phase transition depends primarily on the ratio  $m_H/m_A$  between the scalar and the gauge field mass. For superconductors, these mass scales correspond to the inverse correlation length and the inverse London penetration depth, respectively. For small values of the Higgs field mass the phase transition is strongly enough first order to cut-off long range fluctuations. This corresponds to the good type-I region for standard superconductors,  $m_H/m_A < 1$ . On the other hand, the type-II region corresponds to  $m_H/m_A > 1$ . Here, it is expected that the phase transition changes from first to second order.

A proper treatment of the long range fluctuations is decisive for an understanding of the  $U(1)$ -Higgs phase transition as they change the effective interactions between the fields. The ‘microscopic’ physics in the ultra-violet is characterised by the couplings at the short distance length scale  $1/\Lambda$  (or  $\sim 1/T$ , with  $T$  the temperature). In turn, the physics close to a first-order phase transition depends typically on the (small) photon mass  $m_A$ , and thus requires the knowledge of the couplings at scales  $\ll T$ .<sup>1</sup>

A field-theoretical approach which in principle is able to deal with the effects of long range fluctuations and which describes the related scaling of the couplings is given by the Wilsonian renormalisation group [3–6]. This procedure is based on integrating-out infinitesimal momentum shells about some ‘coarse-graining’ scale  $k$  within a (Euclidean) path-integral formulation. The infra-red effective theory obtains upon integrating the resulting flow w.r.t.  $k \rightarrow 0$ . This way, the characteristic scaling behaviour (or ‘running’) of the couplings as functions of  $k$ , and in particular the running of the Abelian charge  $e(k)$ , is taken into account. A Wilsonian approach thus improves on perturbative resummations in that the perturbative expansion parameter  $e^2 T/m_A$  becomes now scale dependent,  $e^2(k)T/m_A(k)$ . While the former diverges close to a second-order phase transition where the photon mass vanishes, the latter remains finite in the infra-red even for  $m_A(k) \rightarrow 0$  due to the non-trivial scaling of the Abelian charge. The crucial role of running couplings in finite temperature phase transitions has been discussed in pure scalar theories [7,8].

In the present article we employ the Wilsonian renormalisation group to the type-I regime of the  $U(1)$ -Higgs phase transition. Our main contributions are two-fold. First, we take into account the non-trivial scaling of the Abelian charge  $e^2(k)$ , characterized by an effective Abelian fixed point which is kept as a free parameter. The infra-red effects lead the

---

<sup>1</sup>When speaking of ‘scales’ we have always ‘mass scales’ or ‘momentum scales’  $\sim k$  in mind. The corresponding ‘length scales’ are given as  $\sim k^{-1}$ .

Abelian gauge coupling to cross-over<sup>2</sup> from its slow logarithmic running in the ultra-violet (effectively  $4d$ ) to a strong linear running in the infra-red (effectively  $3d$ ). The characteristic scale for this cross-over depends on the precise infra-red (IR) behaviour of the Abelian charge, and is decisive for both the strength of the transition and the properties of the phase diagram. This is currently the least well understood part of the problem. Equally important is to retain the full field dependence of the effective potential (no polynomial approximation), for which an analytical expression is given in the sharp cut-off case. We obtain all thermodynamical quantities related to the first-order phase transition and study their dependence on the cross-over behaviour. Second, we present a detailed quantitative analysis of the ‘coarse-graining’ dependence of our results. This is an important consistency check for the method and the approximations involved. We give quantitative evidence for an intimate link between a truncation of the effective action, and the dependence on the coarse graining scheme, which can simply be displayed as additional ‘error-bars’ due to the scheme dependence.

The  $3d$   $U(1)$ -Higgs phase transition has been studied previously using flow equations [9–13], and within perturbation theory [14–16]. Recent results from lattice simulations for both type-I and type-II regions have been reported as well [17,18]. In [9], the RG flow has been studied for the type-II regime within a local polynomial approximation for the effective potential about the asymmetric vacuum up to order  $\phi^8$  in order to establish the phase diagram, the relevant fixed points and the related critical indices. The polynomial approximation is expected to give reliable results for the scaling solution close to a second-order fixed point. The type-I regime has been discussed for the full potential, using a matching argument for the running of the Abelian charge. In [10], the large- $N$  limit and its extrapolation down to  $N = 1$  has been considered as well. It was pointed out that the local polynomial approximation becomes questionable close to a first-order phase transition or a tri-critical fixed point at about  $N \approx 4$  or smaller. This was later confirmed by Tetradis [12], who in addition abandoned the local polynomial approximation. The present study, aiming particularly at the type-I region of the phase diagram, improves on [9,10] in that the full field dependence of the effective potential will be taken into account. A quantitative description of thermodynamical observables at the phase transition requires a good accuracy for the effective potential in the first place. Our study also goes beyond the work of [12] in three important aspects. We study the dependence of physical observables on the value of the effective Abelian fixed point. In addition, explicit analytical solutions to approximate flow equations are given, as well as a discussion of the scheme dependence.

This article is organised as follows. We introduce the Wilsonian flow equations and the particular Ansatz used for the  $U(1)$ -Higgs theory. The flows for the Abelian charge and the free energy are explained, as well as the further approximations involved (Sect. II). We then proceed with the thermal initial conditions as obtained from perturbative dimensional reduction (Sect. III) and a discussion of the phase diagram and the critical line (Sect. IV). This is followed by a computation of all relevant thermodynamical quantities at the first-

---

<sup>2</sup>This cross-over is not to be confused with the qualitatively different ‘cross-over’ observed in the type-II regime of 3+1 dimensional  $SU(2)$ +Higgs theory.

order phase transition as functions of the effective Abelian fixed point, a computation of the corresponding characteristic scales, and a discussion of the approximations made (Sect. V). A quantitative study of the scheme dependence on the main characteristics of the phase transition is given (Sect. VI), followed by a summary and an outlook (Sect. VII). Three Appendices contain some more technical aspects of our analysis.

## II. FLOW EQUATIONS

### A. Wilsonian flows

Wilsonian flow equations are based on the idea of a successive integrating-out of momentum modes of quantum fields within a path-integral formulation of quantum field theory [3,4]. This procedure, in turn, can also be interpreted as the step-by-step averaging of the corresponding fields over larger and larger volumes, hence the notion of ‘coarse-graining’. The modern way of implementing a coarse-graining within a path-integral formalism goes by adding a suitable regulator term  $\sim \int \phi R_k(q) \phi$ , quadratic in the fields, to the action [5]. This additional term introduces a new scale parameter  $k$ , the ‘coarse graining’ scale. A Wilsonian flow equation describes how the coarse grained effective action  $\Gamma_k$  changes with the scale parameter  $k$ , relating this scale dependence to the second functional derivative of  $\Gamma_k$  and the scale dependence of the IR regulator function  $R_k$ . The boundary conditions for the flow equation are such that the flow relates the microscopic action  $S = \lim_{k \rightarrow \infty} \Gamma_k$  with the corresponding macroscopic effective action  $\Gamma = \lim_{k \rightarrow 0} \Gamma_k$ , the generating functional of 1PI Green functions.

To be more explicit, we follow the ‘effective average action’ approach as advocated in [5] and consider the flow equation

$$\frac{\partial}{\partial t} \Gamma_k[\Phi] = \frac{1}{2} \text{Tr} \left\{ \left( \Gamma_k^{(2)}[\Phi] + R_k \right)^{-1} \frac{\partial R_k}{\partial t} \right\}. \quad (2.1)$$

Here,  $\Phi$  denotes bosonic fields and  $t = \ln k$  the logarithmic scale parameter. The length scale  $k^{-1}$  can be interpreted as a coarse-graining scale [6]. The right hand side of eq. (2.1) contains the regulator function  $R_k$  and the second functional derivative of the effective action with respect to the fields. The trace denotes a summation over all indices and integration over all momenta. The above flow interpolates between the classical and quantum effective action due to some properties of the regulator functions  $R_k$  (see Sect. VIB). It is important to realise that the integrand of the flow equation (2.1), as a function of momenta  $q$ , is peaked about  $q^2 \approx k^2$ , and suppressed elsewhere. Consequently, at each infinitesimal integration step  $k \rightarrow k - \Delta k$  only a narrow window of momentum modes contribute to the change of  $\Gamma_k \rightarrow \Gamma_{k-\Delta k}$ . In particular, modes with momenta  $q \gg k$  do no longer contribute to the running at the scale  $k$ . It is this property which justifies the interpretation of  $\Gamma_k$  as a coarse-grained effective action with modes  $q \gg k$  already integrated out.

For gauge theories, the flow equation (2.1) has to be accompanied by a modified Ward identity which has to be satisfied at each scale  $k$ . Such a requirement is necessary to guarantee that the physical Green functions obtained for  $k \rightarrow 0$  obey the usual Ward identity [19–22]. Here, we use the background field formalism, as employed in [6] in the context of the effective

average action with a covariant gauge fixing (Landau gauge).

The flow equation couples the infinite number of operators describing an effective action with its second functional derivative. In order to solve (2.1), one has to truncate  $\Gamma_k$  to some finite number of operators relevant for the problem under investigation. Some systematic expansions for the flow equations are known. Apart from a weak coupling expansion, which is known to reproduce the standard perturbative loop expansion, one can use expansions in powers of the fields, derivative expansions, or combinations thereof. These latter expansions have the advantage of not being necessarily restricted to a small coupling regime. A discussion on the use of a derivative expansion in Wilsonian RG is presented in [23].

We now turn to our Ansatz for the Abelian Higgs model. The most important information regarding the phase structure of the model is encoded in the effective potential (or coarse grained free energy)  $U_k$ , from which all further thermodynamical quantities are derived. Equally important is the wave function renormalisation factor of the gauge fields  $Z_F$ , which encodes the non-trivial running of the Abelian charge. In turn, the wave function renormalisation factor  $Z_\varphi$  for the scalar fields is less important because the scalar field anomalous dimension remains small in the type-I region of phase transitions. Hence, we approximate the effective action  $\Gamma_k$  to leading order(s) in a derivative expansion through the following operators

$$\Gamma_k[\phi, A] = \int d^d x \left\{ U_k(\bar{\rho}) + \frac{1}{4} Z_{F,k} F_{\mu\nu} F_{\mu\nu} + Z_{\varphi,k} (D_\mu[A]\varphi)^* D_\mu[A]\varphi \right\} \quad (2.2)$$

where  $\bar{\rho} = \varphi^* \varphi$ ,  $F_{\mu\nu} = \partial_\mu A_\nu - \partial_\nu A_\mu$  is the field strength of the electromagnetic field, and  $D_\mu$  denotes the covariant derivative  $\partial_\mu - i\bar{e}A_\mu$ .

In principle, the flow equation can be used directly (starting with initial parameters of the  $4d$  theory at  $T = 0$ ) to compute the corresponding critical potential at finite temperature within the imaginary time formalism, or, like in [24], using a real-time formulation of the Wilsonian RG [25]. Our strategy in the present case is slightly simpler. We are interested in the region of parameter space where the  $4d$  couplings are small enough to allow a perturbative integrating-out of the super-heavy and heavy modes, i.e. the non-zero Matsubara modes for all the fields and the Debye mode. In this case, we can rely on the dimensional reduction scenario and employ the results of [26], who computed the initial conditions perturbatively. The result is then a purely three-dimensional theory for the remaining light degrees of freedom, whose infra-red behaviour is then studied applying the above Wilsonian renormalisation group. In the sequel, we will therefore need the flow equations for  $U_k$  and  $e^2(k)$  in  $3d$ . At the scale of dimensional reduction, that is the starting ultra-violet (UV) scale  $\Lambda$  of the  $3d$ -flow, we normalize the wave function factors to one, and the initial effective potential  $U_\Lambda$  is obtained from dimensional reduction.

## B. Cross-over of the gauge coupling

We now consider the case  $d = 3$ , and discuss the flow for the Abelian coupling. A main feature of the Abelian Higgs theory in  $3d$  is that the Abelian charge scales in a non-trivial manner with the coarse graining scale  $k$ . The dimensionless Abelian charge in  $3d$  is defined as

$$e_3^2(k) = \frac{\bar{e}_3^2(\Lambda)}{Z_F(k)k} \equiv \frac{\bar{e}_3^2(k)}{k}, \quad (2.3)$$

and its scale dependence is related to the gauge field anomalous dimension  $\eta_F = -\partial_t \ln Z_F(k)$  (here a function of  $k$  and the fields) through [6]

$$\frac{de_3^2}{dt} = -e_3^2(1 - \eta_F). \quad (2.4)$$

The first term in (2.4) comes from the intrinsic dimension of the charge squared (proportional to  $k$ ), while the second term proportional to the gauge field anomalous dimension accounts for the non-trivial running of the coupling. The flow (2.4) has always the (trivial) Gaussian fixed point given by  $e_3^2 = 0$ . In addition, one might encounter further non-trivial fixed points which are given implicitly through the solutions of  $\eta_F = 1$ .

Both the scalar and the gauge field anomalous dimensions  $\eta_\varphi$  and  $\eta_F$  are perturbatively small near the Gaussian fixed point, i.e.  $|\eta_\varphi|$  and  $|\eta_F| \ll 1$ . This holds true at the initial scale for  $k = \Lambda$  in the effective  $3d$  running to be specified later. It follows that the running of the dimensionful Abelian charge is negligible near the Gaussian fixed point,  $\bar{e}^2(k) \approx \bar{e}^2(\Lambda)$ . Here, the dimensionless coupling scales as  $e_3^2(k) \sim \Lambda/k$ . In this regime it is expected that standard perturbation theory gives a reliable estimate of the effective potential in this region of the parameter space [13].

However, for  $\eta_F < 1$  the Gaussian fixed point is IR unstable, as follows directly from (2.4). Therefore, when approaching the infra-red, the dimensionless Abelian charge will unavoidably grow large, scaling away from the Gaussian fixed point. In particular, it can enter into a region where  $\eta_F(e^2)$  is no longer  $\ll 1$ . When a non-trivial fixed point is approached, i.e.  $\eta_F \approx 1$ , the suppression factor  $(1 - \eta_F)$  in (2.4) becomes important. A strong linear running of  $\bar{e}^2 \sim k$  (the IR region is effectively  $3d$ ) will ultimately set in as soon as the deviation from the Gaussian fixed point becomes sizeable [9,10,27]. In this regime, we expect some quantitative modifications of the predictions by perturbation theory due to the non-trivial running of the Abelian charge.

### C. Abelian fixed point

The anomalous dimension  $\eta_F$  has been calculated in [6]. It is, in general, a complicated function of the gauge coupling, the fields, and the further parameter describing the effective action in a given approximation, like the coarse grained potential (cf. (113) of [9]). However,  $\eta_F$  is proportional to  $e_3^2$  itself, and we write it as

$$\eta_F(\bar{\rho}) = \frac{e_3^2}{e_\star^2(\bar{\rho})}. \quad (2.5)$$

Given the anomalous dimension, (2.5) provides a definition of  $e_\star^2(\bar{\rho})$ . Our current understanding of the IR behaviour of the gauge sector hinges on the precise properties of  $\eta_F(\bar{\rho})$ , and hence of  $e_\star^2(\bar{\rho})$ .

Let us recall a few cases where  $e_\star^2$  is approximately known. First, within standard perturbation theory, the dimensionful gauge coupling  $\bar{e}_3^2 = e_3^2 k = \text{const}$  throughout. Within our

formalism, the ‘no-running’ corresponds to the limit  $e_\star^2 \rightarrow \infty$ . In this limit, the effective fixed point is independent of the fields and we can expect to be close to the results from perturbation theory, as long as additional effects due to the scalar anomalous dimension can be neglected.<sup>3</sup>

Second, consider the large- $N$  limit of the  $U(1)$ -Higgs model, where  $N$  denotes the number of complex scalar fields. In this limit, the flow (2.4) is dominated by the contributions of the Goldstone modes. They overwhelm those due to the radial mode. Therefore,  $e_\star^2$  becomes

$$e_\star^2 \approx \frac{6\pi^2}{N} \quad (2.6)$$

close to the minimum of the effective potential.<sup>4</sup> In particular, (2.6) does no longer depend on the quartic scalar coupling or the location of the v.e.v. because the massive (radial) mode is suppressed. Extrapolating (2.6) down to the physically relevant case  $N = 1$  corresponds to replacing the radial mode by a massless one. This yields  $e_\star^2 \approx 6\pi^2$  in accordance with the leading order result from the  $\epsilon$ -expansion. This value serves as a reference value for our subsequent considerations.

Third, we recall the findings of [9] and [10], where the function  $\eta_F$  has been studied numerically for different  $N$  within a local polynomial approximation of the flow about the non-trivial minimum at  $\bar{\rho} = \bar{\rho}_0$  (up to  $\sim \phi^8$ ). It was found that the implicit solutions to  $\eta_F(e_\star^2) = 1$  for small  $N$  (in particular  $N = 1$ ) can deviate considerably from the large- $N$  extrapolation  $6\pi^2$ . This deviation is due to the decoupling effects of the massive mode. Still, the qualitative form of (2.5), where the function  $e_\star^2$  is replaced by an effective field-independent fixed point, remains a good approximation to (2.5). This simplified picture persists if the field derivatives  $\partial \ln[e_\star^2(\bar{\rho})]/\partial \bar{\rho}$  remain small within the non-convex region of the effective potential (see also the discussion in Sect. V E). This implies that the threshold effects of the radial mode for  $N = 1$  act on (2.4) as varying the number of scalar fields in (2.6).

Hence, the qualitative structure of the flow (2.4), to leading order, is determined by (2.5) with  $e_\star^2$  given by some number, *e.g.* the appropriate effective fixed point. For the present purpose it is sufficient to study the flow (2.4) with  $e_\star^2$  as a free parameter. The properties of the first-order phase transition depend on the size of  $e_\star^2$ . However, as we shall see in detail below, the dependence turns out to be very small for large  $e_\star^2$ : this part of the phase diagram can be studied without having a complete understanding of the underlying fixed point structure. In turn, we find a strong dependence within regions where the effective fixed point is small. For this case, a more refined analysis is required in order to provide more reliable predictions.

---

<sup>3</sup>In the region where  $\lambda \gg e^2$  (e.g. strongly type-II superconductors), the critical behaviour of the limit  $e_\star^2 \rightarrow \infty$  corresponds to an effective scalar theory which belongs to a different universality class than the  $O(2N)$  scalar theory obtained for  $e_\star^2 \rightarrow 0$  [9].

<sup>4</sup>In (2.6), ‘ $\approx$ ’ means equality up to a regulator scheme dependent coefficient of  $\mathcal{O}(1)$ .

### D. Cross-over scale

Within the remaining part of the article we approximate the anomalous dimension as described above. Hence, the eqs. (2.4) and (2.5) are easily solved by

$$e_3^2(k) = \frac{e_\star^2}{1 + k/k_{\text{cr}}} . \quad (2.7)$$

We note the appearance of a characteristic *cross-over scale*

$$k_{\text{cr}} = \frac{\Lambda e_3^2(\Lambda)}{e_\star^2 - e_3^2(\Lambda)} . \quad (2.8)$$

It describes the cross-over between the Gaussian and the Abelian fixed point, and depends on the initial conditions. For  $k > k_{\text{cr}}$  the running is very slow and dominated by the Gaussian fixed point,  $\bar{e}_3^2(k) \sim \text{const}$ . This corresponds also to the limit  $e_\star^2 \rightarrow \infty$ . On the other hand, for  $k < k_{\text{cr}}$  the running becomes strongly linear and the Abelian fixed point governs the scale dependence,  $\bar{e}_3^2(k) \sim k$ . The question as to how strong the first-order phase transition is affected by this cross-over depends on whether the cross-over scale is much larger (strong effect) or much smaller (weak effect) than the typical scales of the transition (see Sect. VD).

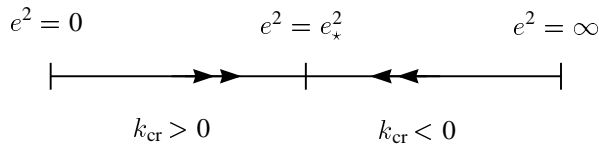


FIG. 1. The relation between the sign of the cross-over scale  $k_{\text{cr}}$  and the running of the gauge coupling (arrows indicate the direction of the  $e^2$  flow as  $k \rightarrow 0$ ).

The cross-over scale turns negative if the initial value  $e_3^2(\Lambda)$  is too big. This simply means that the flow would never be dominated by the Gaussian fixed point (see Fig. 1) in the first place (no cross-over). Although this case is interesting in its own right, this region will not be discussed any further.

### E. The running potential

We now turn to the flow equation for the effective potential, which can be obtained from the flow equation (2.1) using the Ansatz given by (2.2). The resulting flow equation is a second-order non-linear partial differential equation. It has been derived originally in [6] and reads in  $3d$

$$\frac{4\pi^2}{k^2} \frac{d}{dk} U_k(\bar{\rho}) = (2N - 1) \ell_0^3 \left( \frac{U'_k(\bar{\rho})}{k^2} \right) + \ell_0^3 \left( \frac{U'_k(\bar{\rho}) + 2\bar{\rho}U''_k(\bar{\rho})}{k^2} \right) + 2 \ell_0^3 \left( \frac{2\bar{e}_3^2(k)\bar{\rho}}{k^2} \right) \quad (2.9)$$

for the case of  $N$  complex scalar fields. Similar flow equations are obtained for the wave function factors  $Z_\varphi$  and  $Z_F$ , and thus for the anomalous dimensions  $\eta_\varphi = -\partial_t \ln Z_\varphi$  and  $\eta_F = -\partial_t \ln Z_F$ . Here,  $\ell_0^3(\omega)$  denotes a scheme dependent threshold function defined as



$$\ell_n^d(\omega) = -(\delta_{n,0} + n) \int_0^\infty dy \frac{r'(y)y^{1+\frac{d}{2}}}{[y(1+r) + \omega]^{n+1}}. \quad (2.10)$$

These functions have a pole at some  $\omega < 0$  and vanish for large arguments. The function  $r(q^2/k^2)$  is related to the regulator function  $R_k$  introduced in (2.1) through

$$R_k(q^2) = Z q^2 r(q^2/k^2), \quad (2.11)$$

where  $Z$  denotes either the scalar or gauge field wave function renormalisation.<sup>5</sup>

We can distinguish three different contributions to the running of the potential (2.9) which are, from the left to the right, related to the massless scalar, massive scalar, and the gauge field fluctuations, respectively. Not all the three of them are of the same order of magnitude, though. Indeed, it was already noted [28] that the gauge field fluctuations dominate (2.9) if the quartic scalar coupling  $\lambda$  is much smaller than the gauge coupling squared,  $\lambda/e^2 \ll 1$ . This is the case for the physically relevant initial conditions, that is, for the starting point of the flow equation (2.9). Therefore, we can make a further approximation and neglect the contributions from the scalar field fluctuations compared to those from the gauge field. The flow equation thus takes the form

$$\frac{2\pi^2}{k^2} \frac{d}{dk} U_k(\bar{\rho}) = \ell_0^3 \left( \frac{2\bar{e}_3^2(k)\bar{\rho}}{k^2} \right). \quad (2.12)$$

Integrating the approximated flow equation allows to control self-consistently whether the effects from scalar fluctuations remain negligible or not. It suffices to evaluate the right-hand side of (2.9) with  $U_k$  from the solution of (2.12) to compare the contribution of the neglected terms to the running of, say,  $U_k''$  with the leading contributions. It is well known that the scalar fluctuations are important for the inner part of the effective potential which becomes convex in the limit  $k \rightarrow 0$  [29]. Therefore it is to be expected that this approximation becomes unreliable, within the non-convex part of the potential, at some scale  $k_{\text{flat}}$ .

The solution to (2.12) is the first step of a systematic iteration to compute the solution to (2.9). The next step would be to replace  $U_k$  on the r.h.s. of (2.9) by the solution to (2.12). Proceeding to the next iteration step the scalar fluctuations are eventually taken into account. Solving (2.9) with  $U_k$  on the right-hand side replaced by the explicit solution of (2.12) is much easier than solving (2.9) directly, because the former becomes an ordinary differential equation, while the later is a partial one. This procedure can be interpreted as an expansion in terms of scalar loops around the gauge field sector. We will mainly use the first step in the sequel. In order to estimate the integrated contribution of the scalar fluctuations, we will in addition discuss the solution of (2.9) with  $U_k$  on the right-hand side replaced by  $U_\Lambda$  (see Appendix C).

---

<sup>5</sup>A more detailed discussion of both  $R_k$  and the dimensionless functions  $r(q^2/k^2)$  is postponed until Sect. VIB.

## F. The coarse-grained free energy

The coarse grained free energy obtains as the solution to the coupled set of flow equations (2.4) and (2.9). In the present case, a solution can be written as

$$U_k(\bar{\rho}) = U_\Lambda(\bar{\rho}) + \Delta_k(\bar{\rho}) . \quad (2.13a)$$

Here, the term  $\Delta(\bar{\rho})$  stems from integrating out the  $3d$  fluctuations between the scales  $\Lambda$  and  $k$ . With  $e_3^2(k)$  from (2.7) and  $dU_k/dk$  from (2.12), it reads

$$\Delta_k(\bar{\rho}) = \frac{1}{2\pi^2} \int_k^\Lambda d\bar{k} \int_0^\infty dy \frac{r'(y) y^{5/2} \bar{k}^3 (1 + \bar{k}/k_{\text{cr}})}{y \bar{k} (1+r) (1 + \bar{k}/k_{\text{cr}}) + 2e_*^2 \bar{\rho}} + \text{const.} \quad (2.13b)$$

The constant is fixed by requiring that  $\Delta_k(0) = 0$ . In Eq. (2.13b) we see that the term resulting from integrating-out  $3d$  effective modes depends on the RS through the regulator function  $r(y)$  and its first derivative. (Explicit expressions are given in the Appendix B).

The above expressions are enough to study all properties of the phase transitions as functions of the parameters of the potential  $U_\Lambda$ .

We are aiming to use an initial condition at  $k = \Lambda$  obtained from perturbation theory in  $4d$ . This requires that the parametrisation of the  $3d$  potential  $U_\Lambda$  is such that the matching equates the right parameters. In the universal limit  $\Lambda \rightarrow \infty$ , the effective mass term contained via  $U_\Lambda$  is renormalised to  $U_\Lambda \rightarrow U_\Lambda - C_\Lambda \bar{\rho}$ . For a sharp cut-off, we find explicitly

$$C_\Lambda(e) = \frac{e_*^2}{\pi^2} \left( \Lambda k_{\text{cr}} - k_{\text{cr}}^2 \ln(\Lambda/\Lambda_0) \right) . \quad (2.14)$$

For finite  $\Lambda$ , this corresponds to a finite renormalisation of the parameters of the theory, *i.e.* the mass term, or, equivalently, a finite shift of the v.e.v. at the matching scale.<sup>6</sup> This finite renormalisation has its origin simply in the way how the flow equation integrates-out the  $3d$  momentum scales. Only after this transformation it will be appropriate to identify the potential  $U_\Lambda$  at the scale of dimensional reduction with the renormalised effective potential obtained from a perturbative calculation.

## III. THERMAL INITIAL CONDITIONS

We now specify in concrete terms the initial conditions for the effective  $3d$  theory. The task is to relate the  $3d$  renormalised parameters of the effective potential to those of the  $T = 0$   $4d$  theory. The initial conditions for the  $3d$  running are the potential  $U_\Lambda(\bar{\rho})$  and the gauge coupling  $\bar{e}_3^2(\Lambda)$ . The effective perturbative  $3d$  Lagrangean has been derived in [26]. We start with the  $4d$  effective action,

$$\Gamma[\phi, A] = \int d^4x \left\{ \frac{1}{4} F_{\mu\nu} F_{\mu\nu} + (\mathcal{D}_\mu \phi)^\dagger (\mathcal{D}_\mu \phi) - \frac{m_{\text{H}}^2}{2} \phi^\dagger \phi + \frac{\lambda}{2} (\phi^\dagger \phi)^2 \right\} , \quad (3.1)$$

---

<sup>6</sup>This shift corresponds to the finite renormalisation as employed in [12].

where  $\phi$  is a single component  $4d$  complex scalar field. The mass parameter  $m_{\text{H}}$  entering (3.1) denotes the  $T = 0$  Higgs boson mass. It is related to the other zero temperature parameters of the theory by

$$\frac{\lambda}{e^2} = \frac{m_{\text{H}}^2}{M_{\text{W}}^2} \quad (3.2)$$

with  $M_{\text{W}}$  the photon mass. In the phase with spontaneous symmetry breaking,  $m_{\text{H}}^2 > 0$ , we have  $\langle \phi^* \phi \rangle \equiv v^2/2 = M_{\text{W}}^2/2e^2$ . The effective action for the  $3d$  theory obtains as

$$\Gamma_{\Lambda}[\varphi, A] = \int d^3x \left\{ \frac{1}{4} F_{ij} F_{ij} + (\mathcal{D}_i \varphi)^\dagger (\mathcal{D}_i \varphi) + V_{\Lambda}(\bar{\rho}) \right\} , \quad (3.3a)$$

$$V_{\Lambda}(\bar{\rho}) = m_3^2 \varphi^\dagger \varphi + \frac{\bar{\lambda}_3}{2} (\varphi^\dagger \varphi)^2 \quad (3.3b)$$

where  $\varphi$  is the static component of  $\phi$  and  $i, j$  the spatial components of  $\mu, \nu$ . The electric component of the gauge field has been fully integrated out because it acquires a thermal (Debye) mass  $m_{\text{D}}$ . The effects of the fluctuation of this mode are suppressed by inverse powers of  $T$  as  $m_{\text{D}} \propto T$ , like the nonstatic modes. Following [26], the matching conditions read to 1-loop accuracy

$$\bar{e}_3^2(\Lambda) = e^2 T \quad (3.4a)$$

$$\bar{\lambda}_3(\Lambda) = \left( \lambda + \frac{e^4}{4\pi^2} \right) T - \frac{e^4}{4\pi} \frac{T^2}{m_{\text{D}}(\Lambda)} \quad (3.4b)$$

$$m_3^2(\Lambda) = \left( \frac{1}{4} e^2 + \frac{1}{6} \lambda \right) T^2 - \frac{1}{2} m_{\text{H}}^2 - \frac{e^2}{4\pi} T m_{\text{D}}(\Lambda) \quad (3.4c)$$

$$m_{\text{D}}^2(\Lambda) = \frac{1}{3} e^2 T^2 . \quad (3.4d)$$

Using the above, and taking into account the finite renormalisation (2.14) as explained in Sect. II F, the renormalised effective initial potential  $U_{\Lambda}(\bar{\rho})$  entering (2.13a) can be expressed in terms of the  $T = 0$  parameters and (3.4) as

$$U_{\Lambda}(\bar{\rho}) = -m_{\text{R}}^2 \bar{\rho} + \frac{1}{2} \bar{\lambda}_{\text{R}} \bar{\rho}^2 \quad (3.5a)$$

with

$$m_{\text{R}}^2(\Lambda) = \frac{1}{2} m_{\text{H}}^2 - \left( \frac{e^2}{4} + \frac{\lambda}{6} - \frac{e^3}{4\sqrt{3}\pi} \right) T^2 + C_{\Lambda}(e) , \quad (3.5b)$$

$$\bar{\lambda}_{\text{R}}(\Lambda) = \left( \lambda + \frac{e^4}{4\pi^2} - \frac{\sqrt{3} e^3}{4\pi} \right) T , \quad (3.5c)$$

and the dimensionless renormalised quartic coupling reads  $\lambda_{\text{R}} = \bar{\lambda}_{\text{R}}/\Lambda$ . The renormalised v.e.v. at the scale of dimensional reduction follows as

$$\bar{\rho}_{\text{R}}(\Lambda) = m_{\text{R}}^2(\Lambda)/\bar{\lambda}_{\text{R}}(\Lambda) . \quad (3.5d)$$

All the  $3d$  parameters are now defined at the reduction scale  $\Lambda$ , which is on dimensional grounds linearly related to the temperature,

$$\Lambda = \xi T . \quad (3.6)$$

Using eqs. (2.8), (3.4a) and (3.6) it follows, that the cross-over scale  $k_{\text{cr}}$  is also related to  $T$  as

$$k_{\text{cr}} = \frac{\xi e^2}{\xi e_*^2 - e^2} T . \quad (3.7)$$

Let us finally comment on the matching parameter  $\xi$ . On one hand,  $\xi$  has to be smaller than  $2\pi$ , because otherwise the assumption that all heavy modes have been integrated out can no longer be maintained. On the other hand, a too small value for  $\xi$ , say  $\xi < 1$ , would tend to neglect contributions from modes roughly within the window  $\approx 2\pi T$  and  $\approx T$ . For the problem under consideration  $\xi \approx 1$  turns out to be a good choice. This choice shall be adopted throughout. Our results do depend very little on a variation of this matching scale (see also the comment in Sect. V D below).

#### IV. THE PHASE DIAGRAM AT FINITE TEMPERATURE

We have now all the ingredients to study in detail the phase diagram and the phase transition of scalar electrodynamics. In this section, we discuss the main characteristics of the phase diagram as well as some properties of the critical line. The following section collects our results for the thermodynamical quantities related to the first-order phase transition and a discussion of the characteristic scales of the problem.

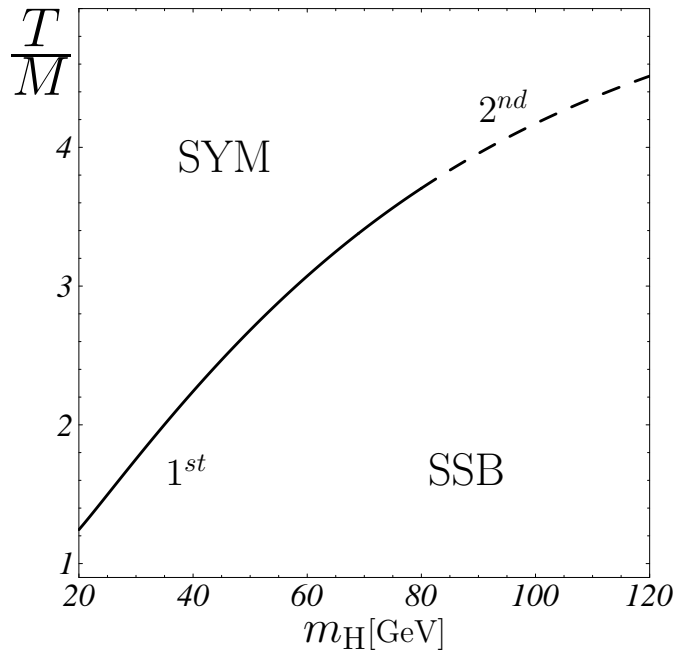


FIG. 2. The phase diagram in the  $(T, m_H)$ -plane.

### A. The phase diagram

The ‘phases’ of scalar electrodynamics are distinguished by the location of the global minimum of the effective potential. Above the critical temperature, the ground state corresponds to vanishing field  $\bar{\rho}_0 = 0$ , that is, to the symmetric phase (SYM). Below the critical temperature, the ground state corresponds to  $\bar{\rho}_0 \neq 0$ , the phase with spontaneous symmetry breaking (SSB).<sup>7</sup> The corresponding phase diagram in the  $(T, m_H)$ -plane is displayed in Fig. 2. The phase transition between these two phases is first order for small  $\bar{\lambda}_3/\bar{e}_3^2$ , that is for small values of the Higgs field mass. In the context of superconductivity this region corresponds to the strongly type-I systems. For very large Higgs field mass, the phase transition turns second or higher order [9].<sup>8</sup>

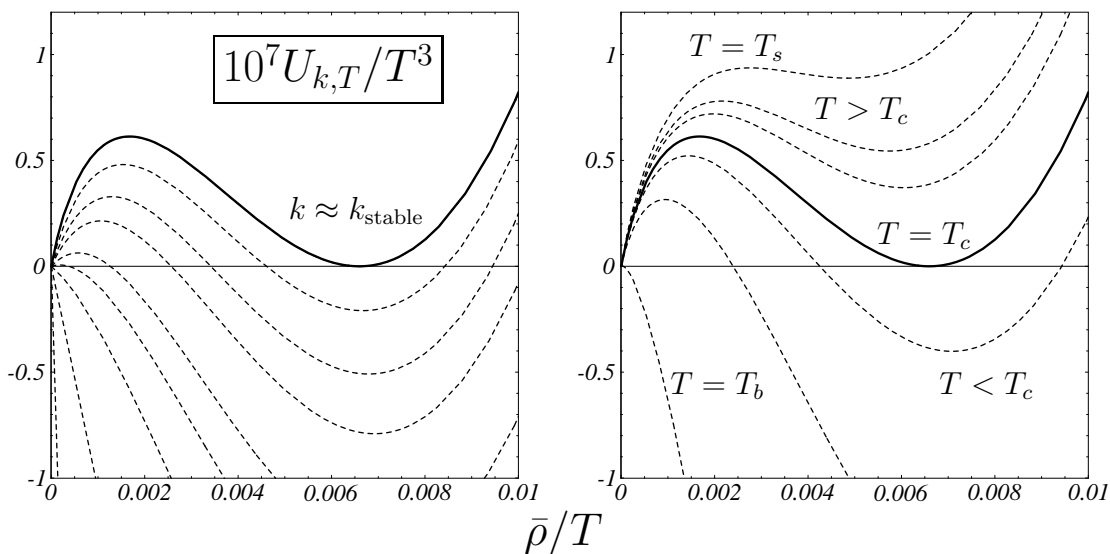


FIG. 3. The coarse grained free energy as a function of the scale parameter and the temperature ( $m_H = 60$  GeV). The full line corresponds to  $T = T_c$  and  $k \approx k_{\text{stable}}$ . Left panel:  $T = T_c$ , for different scales  $k$ . Right panel:  $k \rightarrow k_{\text{stable}}$ , for different temperatures around  $T_c$ .

In Fig. 3, we have displayed the coarse grained free energy within the type-I region of parameters for  $m_H = 60$  GeV for different scales and temperatures. At the critical temperature (left panel), it is realised that a barrier is building up for decreasing scale  $k$ , eventually creating a second minima at vanishing field. The minima are degenerate in the infra-red limit  $k \approx k_{\text{stable}}$  (which corresponds roughly to  $k \rightarrow 0$  in the present approximation). Notice

<sup>7</sup>It is sensible to speak of two distinct phases only for  $N > 1$  complex scalar fields. For  $N = 1$ , the symmetry is never broken in the strict sense. However, we will stick to the usual – albeit slightly incorrect – terminology even for  $N = 1$ .

<sup>8</sup>The strongly type-II region has been studied using flow equations within a local polynomial approximation in [9]. See also [12].

that the flattening of the inner part of the potential is not observed because the scalar fluctuations have been neglected at the present state. Rather, the effective potential reaches the degenerate shape already at some scale  $k_{\text{stable}}$ , which should be larger than the scale where the flattening sets in.<sup>9</sup>

The temperature dependence of the coarse grained free energy at  $k \approx k_{\text{stable}}$  is shown in the right panel. The metastability range  $\Delta T = T_s - T_b$  between the barrier temperature  $T_b$ , where the potential develops a second minimum at the origin (lowest dashed curve) and the spinodal temperature  $T_s$ , where the asymmetric minimum disappears (upper-most dashed curve), is very small.

The physical quantities that characterise a first-order phase transition (except the metastability range) are defined at the critical temperature  $T_c$ , when the potential has two degenerate minima, the trivial one at  $\bar{\rho} = 0$  and a non-trivial one at  $\bar{\rho} = \bar{\rho}_0 \neq 0$ . The critical line of the phase diagram as depicted in Fig. 2 is obtained solving the criticality conditions

$$0 = \left. \frac{dU_k}{d\bar{\rho}} \right|_{\bar{\rho}=\bar{\rho}_0} \quad (4.1a)$$

$$U_k(0) = U_k(\bar{\rho}_0) . \quad (4.1b)$$

Here we kept  $k$  arbitrary though strictly only for  $k = 0$  are these conditions required physically. They establish a relationship between the parameters of the theory, and thereby define the critical line between the symmetric and the SSB phase in Fig. 2. It is helpful to rewrite the conditions (4.1) into

$$F_1(\bar{\rho}/T) = \lambda_R \quad (4.2a)$$

$$F_2(\bar{\rho}/T) = 2 \frac{m_R^2}{T^2} . \quad (4.2b)$$

The functions  $F_1$  and  $F_2$  are related to the fluctuation integral through

$$F_1(x) = \frac{2}{x^2} [\tilde{\Delta}(x) - x\tilde{\Delta}'(x)] \quad (4.3a)$$

$$F_2(x) = \frac{2}{x} [2\tilde{\Delta}(x) - x\tilde{\Delta}'(x)] , \quad (4.3b)$$

with

$$\tilde{\Delta}(\bar{\rho}/T) = \Delta(\bar{\rho})/T^3 . \quad (4.3c)$$

The first condition determines the ratio  $x = \bar{\rho}/T_c$  of the discontinuity to critical temperature in dependence on the  $4d$  parameters as given through  $\lambda_R(e, \lambda)$  from (3.5c). The second one relates the solution of (4.2a) to the ratio of the Higgs boson mass to critical temperature and (3.5b), and eventually to the critical temperature and the discontinuity itself.

Explicit expressions for the scale-dependent effective potential and the function  $\Delta(\bar{\rho})$  are given in the Appendix B.

---

<sup>9</sup>A quantitative discussion of these scales is given in Sect. VD below.

## B. Endpoint of the critical line

Some simple properties of the solutions to (4.2) can be deduced directly from the functions  $F_{1,2}$ . For  $x > 0$ , these functions [with  $\Delta_k$  from (B.5)] are positive, finite, monotonically decreasing and vanishing for  $x \rightarrow \infty$ . They reach their respective maxima at  $x = 0$ , with (for  $k = 0$ )

$$F_1(0) = \frac{2}{\pi^2} e_*^2 e^2, \quad (4.4a)$$

$$F_2(0) = \frac{2}{\pi^2} \frac{\xi^2 e_*^2 e^2}{\xi e_*^2 - e^2} \left( 1 - \frac{e^2}{\xi e_*^2 - e^2} \ln \left( \xi \frac{e_*^2}{e^2} \right) \right). \quad (4.4b)$$

The renormalised  $3d$  quartic coupling  $\lambda_R$ , as given by (3.5c) and fixed through the  $4d$  parameters of the theory, is positive in the domain under consideration. Given the monotony property of  $F_1$  it follows that a solution to (4.2a) is unique (if it exists). There exists no solution for too large values of  $\lambda_R$ . Its largest possible value corresponds to vanishing v.e.v. *i.e.* to  $x = 0$ . Using eqs. (3.2) and (3.5c) gives an upper bound on the scalar mass for the phase transition being first order. It reads

$$\frac{m_H^2}{M_W^2} \leq \frac{2e_*^2}{\pi^2}. \quad (4.5)$$

For any finite value of  $e_*^2$  (4.5) predicts an upper limit for the mass of the Higgs particle. This is an immediate consequence of the existence of an effective fixed point for the running gauge coupling (2.4). Indeed, as the limit  $e_*^2 \rightarrow \infty$  corresponds to perturbation theory we recover the standard perturbative prediction of a first-order phase transition for all Higgs boson mass. This endpoint is usually interpreted as the tri-critical point of the model, above which the phase transition turns from a first-order transition to a second-order one. However, the endpoint of the first-order transition line is within the domain of validity of the present computation only for sufficiently small values of  $e_*^2$ .<sup>10</sup> For larger values of the Abelian fixed point, we expect that the precise location of the endpoint is also determined by the scalar field fluctuations.

In the opposite case, the smallest possible value for  $\lambda_R$  corresponds to  $x \rightarrow \infty$ , thus to  $\lambda_R = 0$ . This gives a lower bound on the mass of the Higgs particle according to

$$\frac{\sqrt{3}e}{4\pi} < \frac{m_H^2}{M_W^2}. \quad (4.6)$$

For  $M_W = 80.6$  GeV and  $e = 0.3$  the bound is satisfied at about  $m_H \approx 16$  GeV. This bound stems entirely from the initial conditions employed. This indicates that the dimensional reduction scenario is no longer appropriate for small  $m_H$ . In the present work, we are also not interested in the region of parameter space where the Coleman-Weinberg mechanism already takes place within the original  $4d$  theory, which happens at even smaller values for  $m_H$  (typically for  $\lambda/e^4$  at about  $3/8\pi^2$  or smaller [27]).

---

<sup>10</sup>The endpoint presented in Fig. 2 corresponds to  $e_*^2 \approx 5$ .

## V. THERMODYNAMICS OF THE FIRST-ORDER PHASE TRANSITION

Here we present our results for the coarse grained free energy and related physical quantities close to the critical temperature of the first-order phase transition as a function of the effective Abelian fixed point. The initial conditions are specified through the gauge coupling at vanishing temperature  $e = 0.3$  and the photon mass  $M_W = 80.6 \text{ GeV}$ . The ratio  $\lambda/e^2$  of the  $4d$  couplings ranges between  $0.06 - 0.75$  for a Higgs field mass between  $20 - 70 \text{ GeV}$ . Relevant information is given by the critical temperature  $T_c$ , the discontinuity at the phase transition  $\bar{\rho}_0$ , the latent heat  $L$  and the surface tension  $\sigma$ .<sup>11</sup> We compare our findings to perturbation theory, and to lattice simulations (for the critical temperature). All our results are obtained as functions of the effective fixed point of the Abelian charge. Due to the approximations performed, they depend also on the regularisation scheme. We use a sharp cut-off regulator throughout the present section. The regularisation scheme dependence is discussed in the following section.

### A. Discontinuity and critical temperature

We begin with the discontinuity and the critical temperature, which follow directly from solving the criticality conditions (4.2).

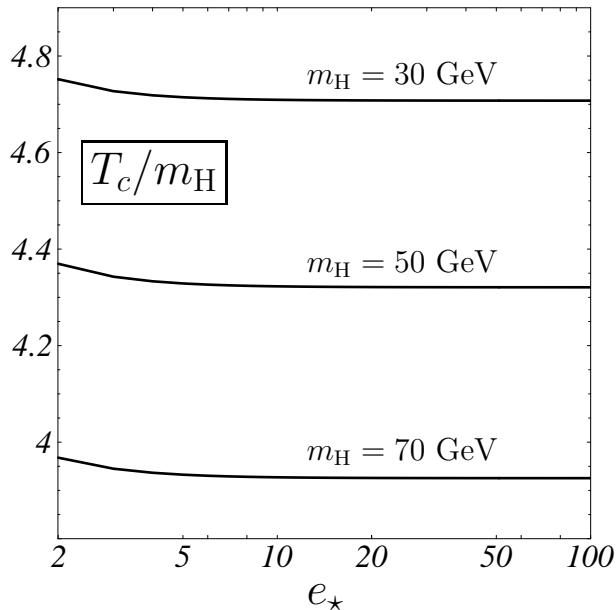


FIG. 4. The critical temperature as a function of the Abelian fixed point.

---

<sup>11</sup>A comment concerning the dimensions is in order:  $U, \sigma, L$  and  $\bar{\rho}$  will be given in  $3d$  units, unless otherwise stated. Their  $4d$  counterparts are simply obtained by multiplying with  $T$ .



The critical temperature as a function of the Abelian fixed point is given in Fig. 4 for  $m_H = 30, 50, 70$  GeV. It turns out that  $T_c$  is rather insensitive against  $e_\star^2$ . We observe an effect of a few percent only for very small values of  $e_\star^2$  (see also Fig. 15). This is not a feature of the Higgs mass being relatively small, as similar results are obtained for all  $m_H$ .

Before continuing, let us briefly compare our findings for the critical temperature to existing lattice data. Lattice results have been reported for  $e = \frac{1}{3}$ ,  $m_W = 80.6$  GeV and  $m_H = 30$  GeV for the non-compact  $U(1)$ -Higgs model in [17], and for the compact one in [18]. The result reported in [17] is  $T_c = 131.18$  GeV for a finite lattice spacing. The continuum limit gives the slightly lower value  $T_c = 130.86$  GeV [18]. This is consistent with  $T_c = 131.28$  GeV, the result for the compact case [18]. Here, for  $e_\star^2 = 6\pi^2$ , we find  $T_c = 128.11$  GeV. As follows from Fig. 4, the critical temperature is essentially independent of the effective Abelian fixed point. The perturbative value is  $T_c = 132.64$  GeV [17]. These results are in good numerical agreement.

We now turn to the discussion of the discontinuity. In Fig. 5 we compare the logarithm of the v.e.v. in  $4d$  units (normalised to the v.e.v. at  $T = 0$ ) at different scales. The renormalisation of  $\bar{\rho}_0$  between the  $T = 0$  and the  $k = \Lambda$  lines results from the integration of the heavy and super-heavy modes, given by (3.5d). The scale  $k_{\text{vev}}$  is defined as the scale where the running of the potential minimum stops. This scale is related to the scale  $k_M$ , where the photon mass in the SSB regime is becoming larger than the coarse graining scale, and thus decouples. Indeed, in the present approximation, the flow equation for the potential minimum reads

$$\frac{d\bar{\rho}_0}{dk} = \frac{1}{\pi^2} \frac{\bar{e}^2(k)}{\bar{\lambda}(k)} \ell_1^3(M^2(k)/k^2). \quad (5.1)$$

Here,  $\bar{\lambda}(k) = U_k''(\bar{\rho}_0(k))$  denotes the quartic coupling at the minimum, and

$$M^2(k) = 2\bar{e}^2(k)\bar{\rho}_0(k) \quad (5.2)$$

the photon mass squared. The running of the v.e.v. decouples at  $k \approx k_{\text{vev}}$ , which happens as soon as the  $3d$  photon mass  $M$  is sufficiently larger than the scale  $k$  (roughly at  $M^2/k^2 \approx 10$ ) such that the threshold function in (5.1) suppresses any further renormalisation ( $k_{\text{vev}}/T$  is displayed in Fig. 12).

From Fig. 5 we conclude that the main part of the actual running of the potential minimum comes from integrating-out the  $3d$  fluctuations, as can be inferred from the wide separation of the  $k = \Lambda$  and the  $k \approx k_{\text{vev}}$  lines as opposed to the comparatively narrow separation of the  $T = 0$  and the  $k = \Lambda$  lines.

Fig. 6 shows the v.e.v.  $\bar{\rho}_0$  as a function of the Higgs field mass and the Abelian fixed point. The shaded region covers the region  $2 \leq e_\star \leq \infty$  for the Abelian fixed point value. For small  $m_H$ , the effect is clearly negligible. With increasing  $m_H$ , however, the influence of the running gauge coupling is increasing drastically, leading to a strong weakening of the phase transition (see also Fig.15).

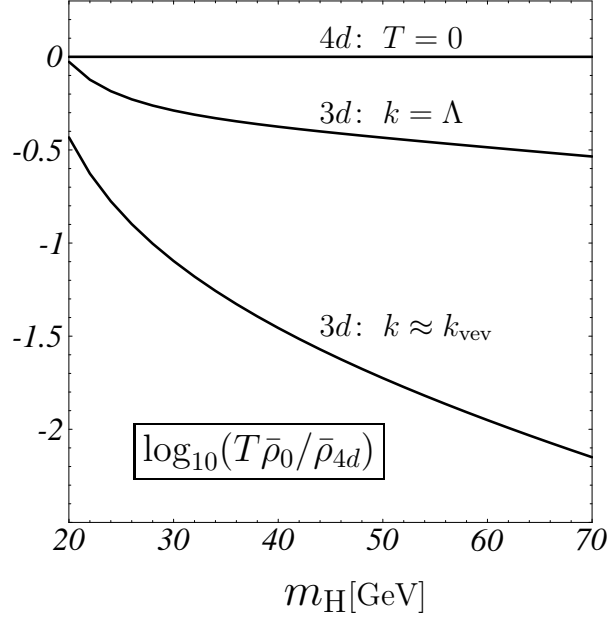


FIG. 5. The size of the v.e.v.  $\bar{\rho}_0(k)$  at  $T = 0$ ,  $k = \xi T$  and at  $k \approx k_{\text{vev}}$  (in units of the  $4d$  v.e.v.  $\bar{\rho}_{4d}$  at  $T = 0$ ).

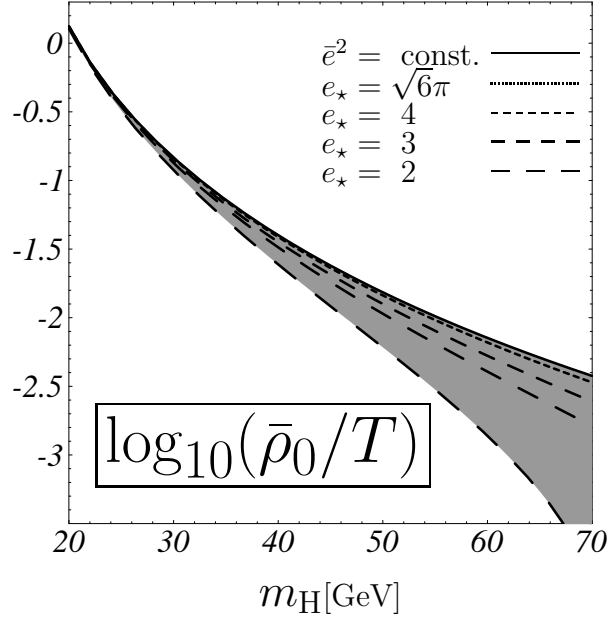


FIG. 6. The  $3d$  v.e.v.  $\bar{\rho}_0$  as a function of the Abelian fixed point.

Finally we compare in Fig. 7 the ratio of the  $4d$  v.e.v.  $\phi_0$  to the initial  $T = 0$  v.e.v.  $v/\sqrt{2}$  for different Abelian fixed point values with the findings of perturbation theory.<sup>12</sup> Again, the

<sup>12</sup>We thank A. Hebecker for providing his data from [15] for comparison in Figs. 7, 9, 10 and 11.

shaded region covers the region  $2 \leq e_* \leq \infty$  for the Abelian fixed point. We observe that the v.e.v. shows a small dependence on the Abelian fixed point for sufficiently small Higgs field mass. For larger values of  $m_H$ , the v.e.v. approaches the perturbative two-loop result. It follows that the v.e.v. is rather stable against effects from the running Abelian charge, say a least for  $e_*^2 > 20$ . Only for  $e_*^2 \approx 4$  the running becomes strong enough to result in a significant decrease of  $\bar{\rho}_0$ .

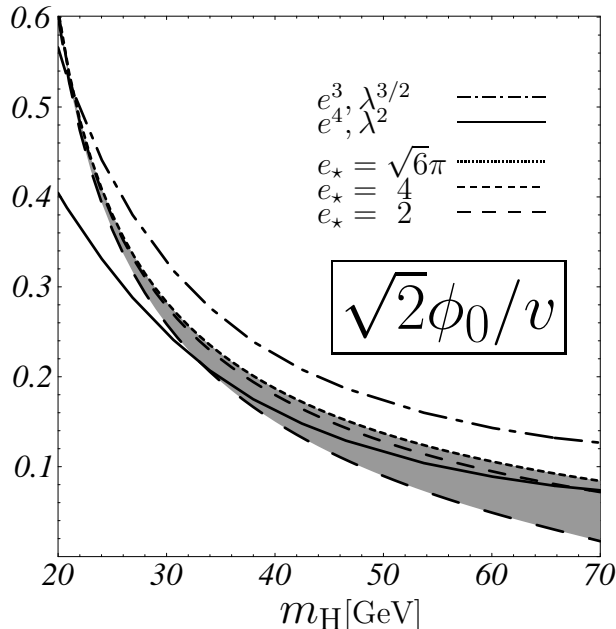


FIG. 7. The v.e.v. for various values of the Abelian fixed point in comparison with perturbation theory to order  $(e^3, \lambda^{3/2})$  and  $(e^4, \lambda^2)$ .

## B. The critical potential

The critical potential is shown in Figs. 8 and 9 for  $m_H = 38$  GeV. Fig. 8 gives the critical potential in units of the critical temperature for different values of  $e_*^2$  as functions of  $\bar{\rho}/T$ .<sup>13</sup> We note that for large  $e_*^2 > 6\pi^2$ , the shape of the potential is rather insensitive against a change in  $e_*^2$ . Here, the additional scale dependence induced through the gauge coupling is quite small (a few percent). For small values of  $e_*^2$ , the height of the barrier is reduced significantly, up to a factor of 3 at  $e_*^2 = 4$ . The strong scaling of  $\bar{e}^2$  thus weakens the phase transition considerably for small  $e_*^2 \ll 6\pi^2$ . Again, the quantitative change depends strongly on the value for the effective Abelian fixed point, if  $e_*^2 \ll 6\pi^2$ . The non-trivial running of  $\bar{e}^2(k)$  has a stronger effect on the small  $\bar{\rho}$  region of the potential. Here, the decoupling of

<sup>13</sup>Notice that comparing critical potentials (or other relevant quantities) in units of  $T$  for different values of  $e_*^2$  is sensible due to the very weak dependence of  $T_c$  on the effective fixed point (see Figs. 4 and 15).

the gauge field sets in only at smaller scales, which in turn results in a stronger quantitative effect due to the running gauge coupling.

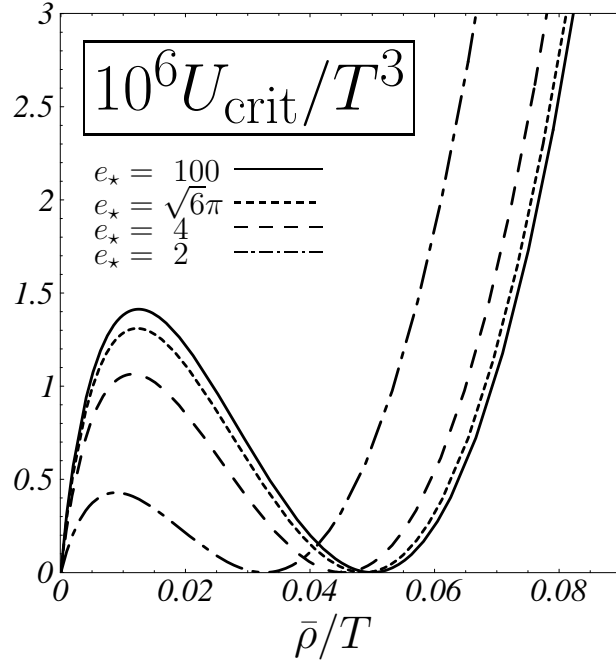


FIG. 8. The critical potential for different values of the effective fixed point.

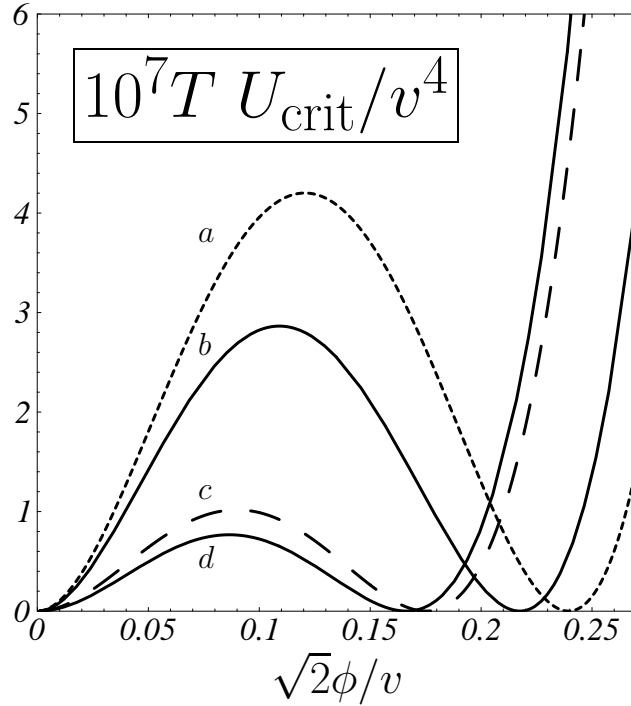


FIG. 9. The critical potential, comparison with perturbation theory (see text).

Fig. 9 gives the critical potential in units of the  $4d$  v.e.v.  $v/\sqrt{2}$ , and compares the solution of (2.12) with those obtained within perturbation theory (PT). Line (a) corresponds to PT to order  $(e^3, \lambda^{3/2})$  [14], line (b) to our result with  $e_*^2 = 6\pi^2$ , line (c) to PT at order  $(e^4, \lambda^2)$  [15] and line (d) to our result with  $e_*^2 = 4$ . For  $e_*^2 = 6\pi^2$ , the critical potential is situated half way between the one- and two-loop perturbative results. For decreasing  $e_*^2$ , the critical potential approaches quickly the two-loop result, and becomes even smaller at about  $e_*^2 \approx 4$ . It is interesting to note that a value for  $e_*^2$  can be found for which the two-loop perturbative result is matched perfectly.

### C. Surface tension and latent heat

The interface tension for a planar interface separating the two degenerate vacua follows from (2.2) as

$$\sigma = 2 \int_0^{\varphi^+} d\varphi \sqrt{Z_\varphi U_{\text{crit}}(\bar{\rho})}. \quad (5.3)$$

It is sensible to the actual shape of the critical potential and yields additional information regarding the strength of the phase transition. In Fig. 10 the surface tension is shown as a function of  $m_H$  and in comparison with perturbation theory. The shaded region covers the results for  $2 \leq e_* \leq \sqrt{6}\pi$ . We again note that the effect of the running coupling is negligible for small Higgs boson mass. In contrast to the v.e.v., the surface tension depends rather strongly on  $e_*^2$  already for moderate values of  $m_H$ . An even stronger running of  $e_3^2$  would lead to a dramatic decrease of the surface tension, up to several orders of magnitude.

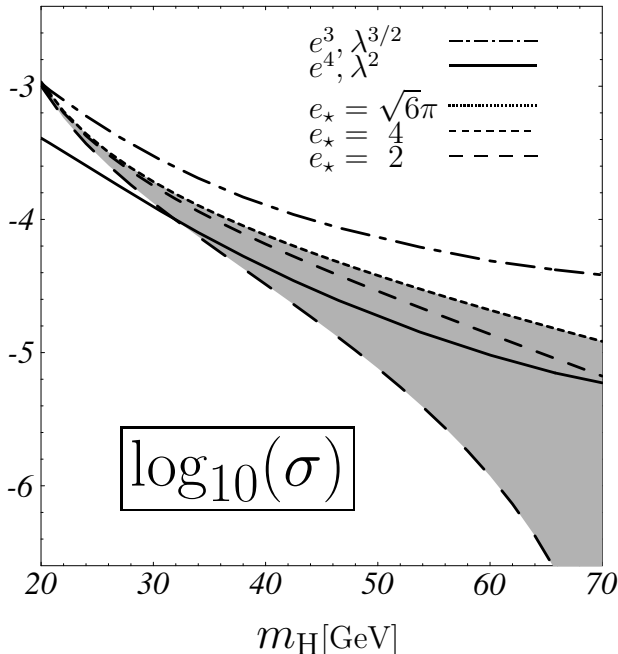


FIG. 10. The surface tension for various values of the Abelian fixed point in comparison with perturbation theory to order  $(e^3, \lambda^{3/2})$  and  $(e^4, \lambda^2)$ .

Finally, we consider the latent heat  $L$ , defined at the critical temperature as

$$L = T \left( \frac{dU(\bar{\rho}_0)}{dT} - \frac{dU(0)}{dT} \right) \Big|_{T=T_c} \quad (5.4)$$

Using eqs. (4.2), (4.3) and (3.5) we obtain

$$L = (m_H^2 - 2m_R^2) \bar{\rho}_0 + \frac{1}{2} \lambda_R T \bar{\rho}_0^2 + 3\Delta(\bar{\rho}_0) - \bar{\rho}_0 \Delta'(\bar{\rho}_0) \quad (5.5)$$

The latent heat is related to the discontinuity and the mass of the scalar particle. Using (4.2), it can be shown that

$$L = \bar{\rho}_0 m_H^2, \quad (5.6)$$

which is also known as the Clausius-Clapeyron equation. This relation was shown to be fulfilled within an explicit gauge-invariant perturbative calculation [16]. However, it holds not true within standard perturbation theory: the perturbative values for the latent heat as found in [15] are all below the value given through the Clausius-Clapeyron relation (5.6). The deviation varies between a few percent up to 15-20% for  $m_H$  between 20 GeV and 70 GeV, and is larger at order  $(e^4, \lambda^2)$  than at order  $(e^3, \lambda^{3/2})$ .

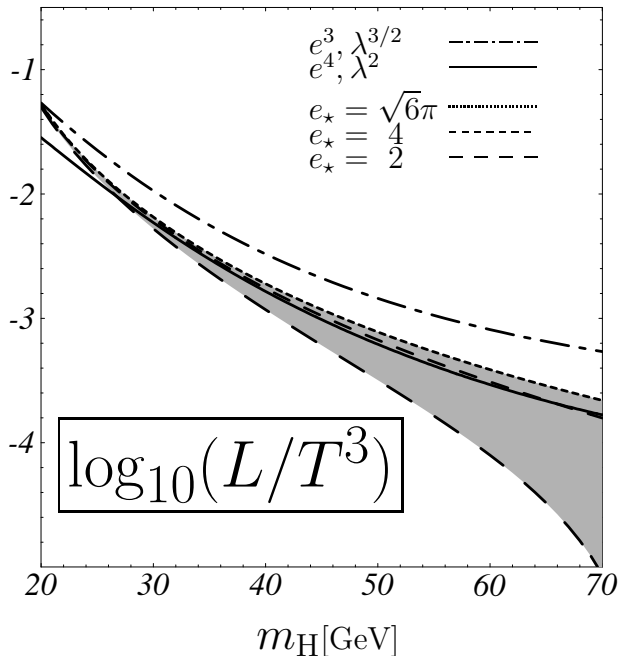


FIG. 11. The latent heat for various values of the Abelian fixed point in comparison with perturbation theory to order  $(e^3, \lambda^{3/2})$  and  $(e^4, \lambda^2)$ .

The latent heat in units of the critical temperature is displayed in Fig. 11 for various values of the effective Abelian fixed point, and in comparison with perturbation theory to order  $(e^3, \lambda^{3/2})$  and  $(e^4, \lambda^2)$ . The shaded region covers the interval  $2 \leq e_\star \leq \sqrt{6}\pi$ . We again observe a sharp decrease for small  $e_\star$  and large Higgs boson mass as in Fig. 7. It is interesting to note that the curve for  $e_\star = 4$  roughly agrees with the two-loop perturbative result for all  $m_H$  above 30 GeV. This is not the case for the surface tension. Comparing Fig. 11 with Fig. 10, we notice that the effect of the running gauge coupling is more pronounced for the surface tension, because the entire region for  $\bar{\rho} \leq \bar{\rho}_0$  enters (5.3), while the latent heat is only affected by  $\bar{\rho}_0$ .

#### D. Characteristic scales

We discuss the results obtained so far in terms of the characteristic scales relevant for the phase transition. Most of the qualitative (and even quantitative) features can be understood once these scales are known.

In Fig. 12, we have depicted the relevant momentum scales as a function of the Higgs mass. The top line at  $k = \Lambda$  corresponds to the scale of dimensional reduction, that is, the starting point of the flow in  $3d$ . The scales  $k_s, k_{\text{vev}}$  and  $k_{\text{stable}}$  (full lines) describe characteristics of the potential, the scale  $k_{\text{cr}}$  (dashed lines, for two values of the Abelian fixed point) the characteristics of the gauge sector, and  $k_{\text{flat}}$  (dashed-dotted line) the scale where scalar fluctuations can no longer be neglected within the non-convex part of the potential. All these scales are now discussed in detail.

At  $k = k_s$ , the origin of the effective potential stabilizes,  $U'(\bar{\rho} = 0) = 0$ , as the mass term squared at vanishing field changes sign. The free energy has two local minima for scales below  $k_s$ . This scale is therefore a good estimate for the scale of discontinuity. In [9], an estimate for this scale has been given, based on a local polynomial approximation for the potential. Within our conventions, it reads  $k_{\text{dis}} \approx 0.18e^4(T)/\lambda_R(T)$  for a sharp cut-off, and roughly coincides with  $k_s$  as presented here ( $k_{\text{dis}}/k_s$  ranges between 1 to 3).

The scale  $k \approx k_{\text{vev}}$  indicates when the v.e.v.  $\bar{\rho}_0$  is within 1% of its final value, eventually reached for  $k \rightarrow 0$ . However, this is not yet the scale where the critical potential has reached a stable shape, which actually happens only at about  $k \approx k_{\text{stable}}$ . This results from the fact that the effective photon mass squared  $2\bar{e}^2(k)\bar{\rho}$  (within the non-convex part of the potential) is smaller than the photon mass at the minimum in the SSB regime (5.2), and the decoupling takes place only at smaller scales. Here, we have obtained  $k_{\text{stable}}$  comparing the depth of the potential  $U(0) - U(\bar{\rho}_0)$  at  $\bar{\rho}_0$  with the height of the barrier  $U(\bar{\rho}_{\text{max}}) - U(0)$ , demanding this ratio to be below  $\approx 5\%$ . At  $k = k_{\text{stable}}$ , the v.e.v. is as close as 0.1% to its final value.<sup>14</sup>

The cross-over scale  $k_{\text{cr}}$  characterises the cross-over from the Gaussian to the Abelian fixed point. For  $e_\star^2 = 6\pi^2$ , we see that  $k_{\text{cr}}$  is about 1-2 orders of magnitude smaller than the scale  $k_s$ , which explains why the running gauge coupling has, in this case, only a small numerical

---

<sup>14</sup>Remember that the critical potential at  $k_{\text{stable}}$ , within the present approximations, is about the same as at  $k = 0$ , as no substantial running takes place below  $k_{\text{stable}}$ .

effect on the properties of the phase transition. From the fact that the scales  $k_{\text{vev}}$  and  $k_{\text{stable}}$  are separated by an order of magnitude ( $k_{\text{vev}}/k_{\text{stable}} \approx 5$ ), we can conclude that the running of the gauge coupling has a stronger effect on physical observables based on the entire effective potential (like the surface tension), than those related only to the v.e.v. (like the latent heat). This is quantitatively confirmed by the findings displayed in the Figs. 6, 7, 10 and 11. For  $e_*^2 = 4$ , we realize that the corresponding cross-over scale is of the same order of magnitude as the scales  $k_s$ ,  $k_{\text{vev}}$  and  $k_{\text{stable}}$ .<sup>15</sup> This is the region where the running of the gauge coupling has a strong quantitative effect on the properties of the phase transition, leading to a significant decrease of the strength of the transition.

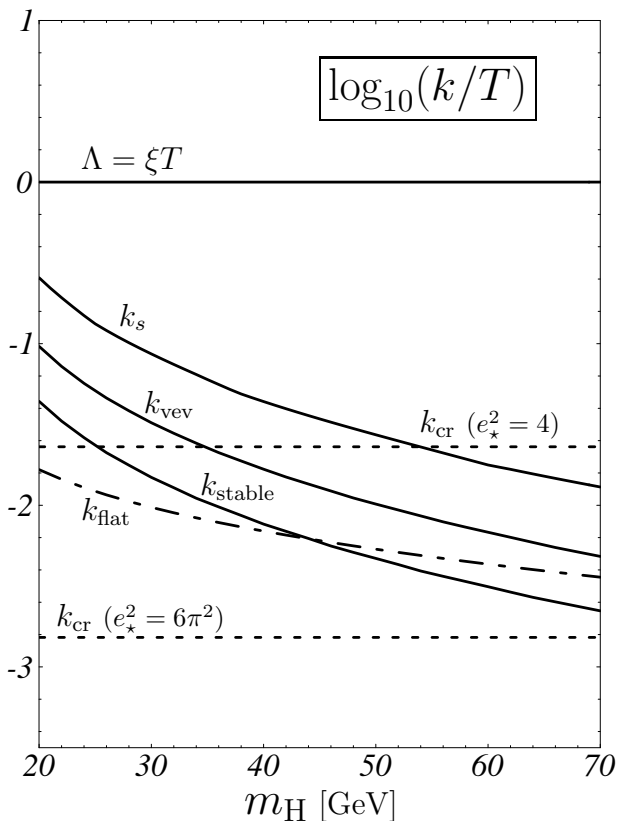


FIG. 12. Characteristic scales (see text).

Finally, we have also indicated the scale  $k_{\text{flat}}$  (dashed-dotted line), which is an estimate for the scale where the flattening of the inner part of the effective potential sets in. We obtained  $k_{\text{flat}}$  from solving  $k^2 + U'_k(\bar{\rho}) \approx 0$  numerically for  $k$  in the non-convex part of the potential,

---

<sup>15</sup>In Fig. 12, the scales  $k_s$ ,  $k_{\text{vev}}$ ,  $k_{\text{stable}}$  and  $k_{\text{flat}}$  have been obtained for  $e_*^2 = 6\pi^2$ . The corresponding results for  $e_*^2 = 4$  do deviate (for larger Higgs mass) only slightly from the curves as presented here. This minor difference is of no relevance for the present discussion.



with  $U_k$  the leading order solution for the free energy.<sup>16</sup>

In [13] an estimate for the ratio of  $k_{\text{flat}}/k_{\text{stable}}$  has been obtained, based on an investigation of the surface tension of the 3d Abelian Higgs model in the universal limit  $\Lambda \rightarrow \infty$ . There, it was found that  $k_{\text{flat}}^2/k_{\text{stable}}^2 \approx \bar{e}^2/M$ , with  $M$  being the 3d photon mass. The boundary  $k_{\text{flat}}^2/k_{\text{stable}}^2 \approx 1$  yields the relation  $k_{\text{flat}} \approx (e^2 T/2\bar{\rho}_0)^{1/4} k_{\text{stable}}$ , which, using the data for  $k_{\text{stable}}$  as in Fig. 12, coincides within a few percent with the line for  $k_{\text{flat}}$  as obtained above. Corrections to the universal limit can be expanded as a series in  $M^2/\Lambda^2$  [13]. In the present case, we start at a finite scale  $\Lambda = \xi T$ , but the smallness of  $M^2/\Lambda^2$  (ranging from 0.2 to 0.001 for  $20 \text{ GeV} \leq m_H \leq 70 \text{ GeV}$ ) is responsible for the small corrections with respect to the universal limit  $\Lambda \rightarrow \infty$ . Being close to the universal limit of the effective 3d theory also explains why the dependence on the matching parameter  $\xi$  is rather small.

We now come back to the discussion of  $k_{\text{flat}}$  from Fig. 12, which, by definition, sets the scale below which the scalar fluctuations trigger the flattening within the non-convex part of the potential, and hence the scale below which these fluctuations should no longer be neglected. First notice, that the scale of discontinuity  $k_s$  is bigger than  $k_{\text{flat}}$  by an order of magnitude. We can thus expect that the scale of discontinuity is only weakly affected by the scalar fluctuations. Also,  $k_{\text{vev}} > k_{\text{flat}}$  by a factor of  $\approx 5$ . Finally, for small Higgs field mass,  $k_{\text{flat}}$  is also smaller than  $k_{\text{stable}}$ . In this region, only small quantitative changes are expected if the scalar fluctuations are taken into account. This is no longer the case for large Higgs field mass, where  $k_{\text{flat}} \geq k_{\text{stable}}$ . However, as these effects concerns mainly the non-convex part of the potential, and thus quantities like the surface tension, we can still expect that the latent heat and the v.e.v. are only moderately affected.

These last observations are also relevant for the applicability of Langer's theory of bubble nucleation. The concept of an interface tension, as defined in (5.3), is based on the implicit assumption that the scale  $k_{\text{stable}}$  can indeed be identified. A criterion for this being the case is the smallness of the perturbative expansion parameter. From our consideration we can conclude that this will become more and more difficult for increasing  $e^2 T_c/2\bar{\rho}_0 \geq 1$ , that is, for very weakly first-order phase transitions.<sup>17</sup>

### E. Higher order corrections

Finally, we comment on the higher order corrections which are expected from operators neglected within the present approximation. Clearly, the results presented here are affected by the approximations performed, most notably through (i) the derivative expansion, (ii) neglecting the scalar field fluctuations as opposed to the gauge field ones, (iii) approximating the infra-red regime of the Abelian charge by an effective fixed point, and (iv) computing the initial conditions perturbatively. We discuss these approximations now one by one.

---

<sup>16</sup>A similar though slightly shifted curve for  $k_{\text{flat}}$  is obtained from solving  $k^2 + U'_k(\bar{\rho}) + 2\bar{\rho}U''_k(\bar{\rho}) \approx 0$ .

<sup>17</sup>The treatment of very weakly first-order transitions based on coarse grained potentials has been considered in [31].

(i) The leading order terms of the derivative expansion are known to correctly describe critical equations of state and scaling solutions for a variety of  $O(N)$ -symmetric scalar models in  $3d$ . Although little is known about the convergence of such an expansion, it appeared that the smallness of the anomalous dimensions controls the influence of higher order derivative operators in the effective action. Therefore, an *a posteriori* consistency check for the reliability of the derivative expansion consists in computing the corresponding scalar and gauge field anomalous dimension  $\eta_\varphi$  and  $\eta_F$ . In the present case, this involves more complicated higher order threshold functions (for their definitions and further details, see [9]). At the scale  $k \approx k_{\text{stable}}$ , we can compute the scalar anomalous dimension self-consistently from the explicit solution for the effective potential, obtained while neglecting  $\eta_\varphi$ . We find that  $|\eta_\varphi| \leq 0.005$  in the interval considered, which is consistent with our initial approximation  $\eta_\varphi = 0$  and justifies the derivative expansion within the scalar sector. For  $N = 1$ , the gauge field anomalous dimension  $\eta_F$  can be estimated in a similar way. It becomes of order one only when the non-trivial fixed point is approached. We find that  $\eta_F$  ranges from 0.03 to 0.4 within the range of Higgs field masses considered here and for  $e_x^2 \approx 6\pi^2$ . A main difference between the scalar and the gauge field sector is that the gauge field anomalous dimension grows large ( $\eta_F = 1$ ) at a scaling solution. Therefore, one expects that higher order corrections within a derivative expansion (or the momentum dependence of the gauge coupling) can become important at a scaling solution and should not be neglected. In the present case, however, the scales relevant for the first-order phase transition have been reached before the Abelian charge finally runs into its non-trivial fixed point, that is before  $\eta_F = 1$ . Therefore we can expect that the derivative expansion behaves reasonably well even for the gauge field sector.

(ii) In the same way, we can check the validity of neglecting scalar fluctuations within the non-convex part of the effective potential. It is found that the self-consistent inclusion of scalar fluctuations to leading order results in corrections of the order of a few percent, increasing with increasing Higgs field mass (see Appendix C). This agrees also with the discussion of the preceding section, where it was argued that scalar fluctuations should no longer be neglected as soon as  $k_{\text{flat}}$  is of the order of  $k_{\text{stable}}$ . Clearly, the weaker the first-order phase transition the more scalar fluctuations will become relevant at the phase transition. For a quantitatively more reliable computation of thermodynamical quantities in the weakly type-I region, one has to go beyond the present approximation and include scalar fluctuations. All the present approximations can be improved in a systematic way, as has been emphasized earlier. This can be done either along the lines outlined in Sect. II E, or by a straightforward numerical integration of the flow equation as in [12].

(iii) The main uncertainty in the present understanding of the  $U(1)$ -Higgs theory is linked to the gauge sector of the theory *i.e.* the precise infra-red behaviour of the Abelian gauge coupling. Here we have effectively parametrised this uncertainty in terms of an Abelian fixed point motivated by previous work based on large- $N$  extrapolations and Wilsonian RG techniques. A precise determination of the correct fixed point requires the study of the momentum and of the field dependence of the Abelian charge. Our approximation assumes that the field gradients of the function  $e_x^2(k, \bar{\rho})$  remain sufficiently small within the non-convex part of the potential at scales above  $k \approx k_{\text{stop}}$ . In the large- $N$  limit, where this fixed point is well understood, the results in the present approximation are in very good agreement with

the result found within a fixed dimension computation.

(*iv*) The points (*i*) – (*iii*) concerned the approximations on the level of the flow equation. These are the most important ones, because they act back on  $\Gamma_k$  upon integration of the flow. An additional approximation concerns the initial conditions to the flow. Here, they have been obtained from the dimensional reduction scenario within a perturbative loop computation. For the present purposes, it was sufficient to use a 1-loop perturbative matching as given in Sect. III, although the 2-loop matching has been reported as well [30]. These higher order effects can be taken into account in principle; in practice, this shall not be necessary because their quantitative influence is smaller than the contributions from the scalar fluctuations for larger Higgs field mass, which have already been neglected. In any case, a small change of the initial condition cannot change the main effect reported here. Except for small Higgs field masses, the dominant contributions come from integrating-out modes in  $3d$ . This follows directly from Fig. 5, which shows that the main running of the v.e.v. takes place below the scale of dimensional reduction.

Finally, we remark that the quality of a given approximation can also be assessed by studying the dependence on the coarse graining scheme. This discussion will be the subject of the following section.

## VI. SCHEME DEPENDENCE

All quantitative results present up to now have been obtained for a sharp cut-off regulator. It is a straightforward consequence of the Wilsonian renormalisation group approach that physical observables obtained from a solution to a Wilsonian flow equation will not depend on the precise form of the coarse-graining. Unfortunately, this conclusion holds only if the *full* effective action is computed. On a technical level, this is barely possible, and truncations of the effective action have to be employed. It is precisely this truncation that can introduce a spurious coarse graining scheme dependence for physical observables. In this section we address the question as to what extend the physical observables as obtained in the preceding section do (or do not) depend on the precise form of the coarse graining. In doing so, we are able to present quantitative ‘error bars’ related to the scheme dependence. We also present evidence for an intimate quantitative link between the scheme dependence and the truncations employed.

### A. Scheme dependence vs. truncations

Consider the case of computing some physical observable from the solution to a (truncated) Wilsonian flow. It goes without saying that a *strong* dependence of this observable on the coarse graining employed is not acceptable as it would cast serious doubts on the truncations performed so far. With ‘strong’ we mean ‘inducing large quantitative’, or even ‘qualitative’ changes. On the other hand, a *weak* scheme dependence of certain physical observables is a sign for the viability of the approximation employed. In fact, if we were able to solve the flow equations without truncating the effective action  $\Gamma_k$ , the final result in the physical limit  $k \rightarrow 0$ , which is by construction nothing else but the full quantum effective action  $\Gamma$ , should not depend on the details of the particular coarse graining employed. There is little

hope for this holding true for any truncation of the effective action  $\Gamma_k$  as any truncation necessarily neglects infinitely many operators.

The coarse graining procedure is implemented through the momentum-dependent operator  $R_k(q^2)$ . It couples to all the operators present in  $\Gamma_k$  in a well-defined way, that is, according to the flow equation (2.1). Replacing a coarse-graining by another coarse graining implies that the effective coupling of  $R_k(q^2)$  to the operators contained in the effective action changes accordingly. A truncation of the effective action amounts to neglecting infinitely many operators to which the coarse graining, in principle, is sensitive. Therefore, studying the scheme dependence will probe whether some relevant operators (for the problem under investigation) have been neglected, or not. In this light, the indirect feed-back of some relevant operators should manifest itself through some strong eigenmode with respect to a change of the coarse graining procedure.

Although these arguments, as presented so far, are of a purely qualitative nature, we will show in the sequel that they can indeed be given a quantitative meaning.

## B. Coarse grainings

Before studying in detail the scheme dependence of our results, we will briefly review the main requirements for a viable coarse graining procedure. There are basically three key points to be considered. The first one concerns the possible zero-modes of the propagators, which typically cause strong infra-red problems within perturbative loop expansions in  $d < 4$  dimensions. These are properly regularised, if

$$\lim_{q^2 \rightarrow 0} R_k(q^2) > 0 \tag{6.1a}$$

holds true. This way, the effective inverse propagator for a massless mode reads  $q^2 + R_k(q^2)$ , and has a well-defined infra-red limit. The second point concerns the infra-red limit of the effective action  $\Gamma_k$ , which should coincide with the usual effective action for  $k \rightarrow 0$ . This is the case, if

$$\lim_{k \rightarrow 0} R_k(q^2) = 0 . \tag{6.1b}$$

Finally, we have to make sure that the correct initial effective action in the ultra-violet limit is approached which is guaranteed by

$$\lim_{k \rightarrow \infty} R_k(q^2) \rightarrow \infty . \tag{6.1c}$$

Any function  $R_k(q^2)$  with the above properties can be considered as a coarse graining [5,13]. It is convenient to re-write  $R_k$  in terms of dimensionless functions  $r(q^2/k^2)$  as

$$R_k(q) = Z q^2 r(q^2/k^2) , \tag{6.2}$$

where  $Z$  corresponds to a possible wave-function renormalisation ( $Z_\phi = 1$  in our approximation).

Let us introduce two classes of regulator functions which are commonly used in the literature. The first one is a class of *power-like* regularisation schemes given by the coarse-graining function

$$r_p(y) = y^{-n} , \quad (6.3)$$

and  $y \equiv q^2/k^2$ . The particular case  $n = 1$  corresponds to a mass-like regulator  $R_k \sim k^2$ , and  $n = 2$  to a quartic regulator  $R_k \sim k^4/q^2$ . These algebraic regulators are often used because the related threshold functions can be computed analytically. On the other hand, these regulators decay only algebraically for large momenta, which can in principle lead to an insufficiency in the integrating-out of the hard UV modes.

A second convenient class of regulators consists of exponential ones, parametrised as

$$r_e(y) = \frac{1}{\exp(cy^n) - 1} , \quad (6.4)$$

where  $c$  is a constant. The exponential regulator with  $n = c = 1$  has been used previously in various numerical investigations [9,10,27]. The suppression of large momentum modes  $q^2 \gg k^2$  to the flow is now exponential and thus much stronger than in the case of algebraic regulators. It is expected that this property is at the basis for a good convergence of approximate solutions.

Both classes of regulator functions depend on the parameter  $n$ , with  $1 \leq n \leq \infty$ . In the limit  $n \rightarrow \infty$ , they both approach to what is known as the sharp cut-off regulator, given by [3,4]

$$r_s(y) = \frac{1}{\theta(y - 1)} - 1 . \quad (6.5)$$

We will now consider the dependence of certain physical observables on particular choices of these regulators.

### C. Tri-critical point and large- $N$ limit

We have given an estimate for the endpoint of the critical line in (4.5). Its mere existence is closely linked to the presence of an Abelian fixed point, although it will be within the domain of validity only for small values of the latter. Both functions  $F_1$  and  $F_2$  depend explicitly on the RS, and so does the solution to eqs. (4.2). In the general case, the endpoint of the critical line also depends on the RS. Instead of (4.5), which is the result for a sharp cutoff, we find for the general case

$$\frac{m_{\text{H}}^2}{M^2} = \frac{8a_1}{3\pi^2} e_*^2 , \quad (6.6)$$

where terms  $\mathcal{O}(e)$  have been dropped. The entire scheme dependence is now encoded in the coefficient  $a_1$ , given by

$$a_1 = -\frac{3}{2} \int_0^\infty dy \frac{r'(y) y^{-\frac{1}{2}}}{[1 + r(y)]^3} \quad (6.7)$$

in  $d = 3$  dimensions. This coefficient belongs to a set of expansion coefficients  $a_k$  characterising a coarse graining scheme (see Appendix A for their general definition and more details). For each of the two classes of regulators the coefficient  $a_1$  can be calculated as a function of the parameter  $n$ . In Fig. 13, the dashed line corresponds to the power-like, and the full line to the exponential regulator class with  $c = \ln 2$ . For this choice of  $c$  both set of regulators are normalised to  $r(1) = 1$ . For a power-like regulator, we find explicitly  $a_1 = \frac{3}{4}\Gamma[1 + \frac{1}{2n}]\Gamma[2 - \frac{1}{2n}]$ , and for the exponential one  $a_1 = \frac{3}{8}n^{-1}c^{1/2n}(2^{1/2n} - 2)\Gamma[-\frac{1}{2n}]$ . It is interesting to note that although these classes of regulators do have strong qualitative differences, the coefficient  $a_1$ , which only involves a folding of  $r(y)$  over all momenta, is rather stable (*i.e.*  $\pm 10\%$  about the mean value).

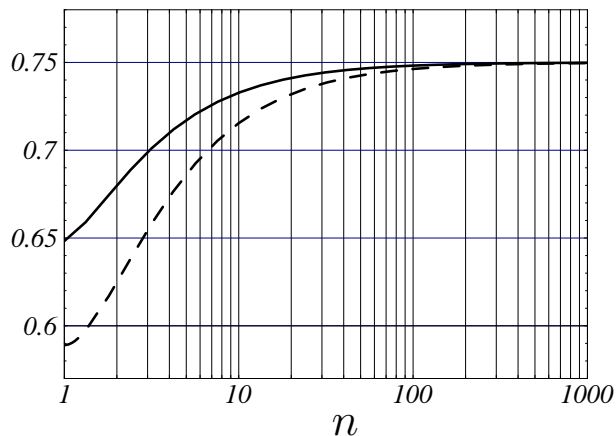


FIG. 13. The expansion coefficient  $a_1$  (see text).

We shall compare the numerical value of the tri-critical point with results obtained in the large- $N$  limit via the  $\epsilon$ -expansion [32] or a fixed dimension computation in ( $d = 3$ ) [33]. As argued in Sect. II B, the Abelian fixed point reads  $e_*^2 = 6\pi^2/N$  in the large- $N$  limit, and our above result therefore becomes

$$\frac{\lambda_3}{e_3^2} = 16a_1 \frac{1}{N} \approx (9.4 - 12.0) \frac{1}{N} \quad (6.8)$$

The  $\epsilon$ -expansion, to leading order, yields

$$\frac{\lambda_3}{e_3^2} = (54 - 136\epsilon) \frac{1}{N} \quad (6.9)$$

This is to be compared to the result of [33], which reads

$$\frac{\lambda_3}{e_3^2} = \frac{96}{\pi^2} \frac{1}{N} \approx 9.9 \frac{1}{N} \quad (6.10)$$

While (6.9) fails to give a reliable answer at  $\epsilon = 1$ , we observe that our result (6.8) is in good numerical agreement with (6.10).

## D. Scheme dependence of the critical potential

Here, we consider the task of computing the critical potential for coarse grainings other than the sharp cut-off. First, we have to obtain the corresponding fluctuation integrals. The most general expression (for arbitrary scheme) has been given in Appendix B. This expression still contains an integral over momenta to be performed, which is how the scheme dependence enters into the expression for the fluctuation integral  $\Delta_k$ . Then, the criticality conditions (4.2) have to be solved to find  $T_c$  and  $\bar{\rho}_0$ . The sharp cut-off allowed an analytical computation of  $\Delta_k$ , (B.5), and thus of the functions  $F_{1,2}$  in (4.3).

Below, in addition to the sharp cut-off, we consider the classes of power-like regulators (6.3) and exponential regulators (6.4). From the power-like regulators, we consider the limiting cases  $n = 1$  (*i.e.* a mass-like regulator  $R_k = k^2$ ) and  $n = \infty$  (the sharp cutoff). As an intermediate case we consider also the case  $n = 2$  (*i.e.* the quartic regulator  $R_k = k^4/q^2$ ). The exponential regulators are represented for  $n = 1$  (*i.e.*  $R_k = q^2/(\exp q^2/k^2 - 1)$ ), and  $n = \infty$  (the sharp cutoff). A continuity argument suggests that the critical potentials for intermediate values of the coarse graining parameter  $n$  should appear within those limits set by  $n = 1, 2$  and  $n = \infty$ .

No explicit analytical expressions for the coarse grained free energy have been found in these cases. For the mass-like and the quartic regulator we used the integrals (B.7) and (B.8), respectively, while (B.2) is used for the exponential regulator. Then, the problem of solving the criticality conditions reduces to the optimization of two integral equations.

We find that the critical temperature  $T_c$  depends very weakly on the different schemes. Indeed, plotting  $T_c$  as a function of the Higgs field mass we find that the lines corresponding to different schemes are almost on top of each other, inducing a relative error well below the 1% level (and thus below the error already present due to other approximations). A similar situation holds for the v.e.v., where we find a relative error below a few percent.

In Fig. 14, the entire critical potential (in units of the  $4d$  v.e.v.) is displayed for different coarse grainings at  $m_H = 38$  GeV (left panel) and at  $m_H = 70$  GeV (right panel). The labels  $s$ ,  $q$ ,  $m$  and  $e$  denote respectively the sharp cut-off, the quartic/mass-like regulator, and the exponential cut-off from (6.4) for  $n = 1$  and  $c = 1$ .

We first consider  $m_H = 38$  GeV, and notice that the  $s$  and  $q$  lines turn out to be on top of each other. Furthermore, it is realised that the v.e.v. is nearly independent on the RS, as is the shape of the potential close to the minima. The main dependence concerns the local maximum of the critical potential. This dependence will therefore affect integrated quantities like the surface tension, but not those related to the v.e.v., like the latent heat. The error for the surface tension in the present case is about a few percent.

For  $m_H = 70$  GeV the dependence on the scheme is more pronounced than in the previous case. Furthermore, the v.e.v. receives – for the mass-like regulator – a sizeable shift towards smaller values. Again, the variance is strongest around the maximum of the critical potential, and dominant in the non-convex region of the critical potential. The additional shift in the value of the v.e.v. entails a corresponding shift for the outer region of the effective potential, as opposed to the case for smaller Higgs field mass.

It is interesting to make contact with the qualitative considerations presented at the be-

ginning of this section, and to compare the scheme dependence observed in Fig. 14 with the reliability of the coarse grained potential in its different regions, due to the approximations employed. Recall that the present computation is based on neglecting the scalar fluctuations. This approximation is more reliable for the outer part of the potential than for the non-convex part of it (more precisely, around a small region of the maximum of the inner part of the potential). Here, scalar fluctuations cause ultimately the flattening of the potential in the IR limit. While we have seen in Sect. VD that this approximation is still reliable for  $m_H = 38$  GeV, we certainly expect larger corrections for  $m_H = 70$  GeV (see the discussion of Sects. VD and VE). It is quite remarkable that the scheme dependence indeed seems to reflect the weakness of the approximation for this region of the potential. Our computation thus turns the qualitative statement into a quantitative one.

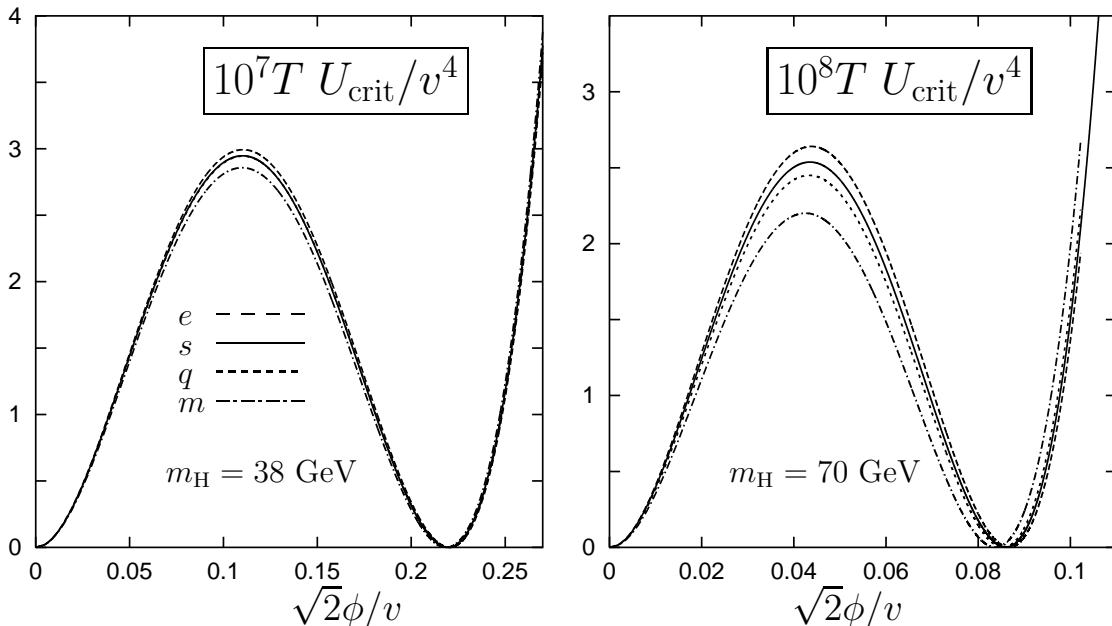


FIG. 14. The critical potential for  $m_H = 38$  GeV (left panel) and  $m_H = 70$  GeV (right panel), and different regulator schemes: exponential regulator (e), sharp cut-off (s), quartic regulator (q) and mass-like regulator (m).

Finally, we briefly comment on the different regulators used. It is well-known that the mass-like regulator is marginal in the sense that it has a poor UV behavior which makes its use for certain applications questionable (a more refined discussion has been given in [22]). From Fig. 14, we learn that the critical potential as obtained for the mass-like regulator deviates the most from the results for the other regulators employed. Considering the class of power-like regulators, we see from Fig. 14 that the width between the quartic and the sharp cut-off limit is significantly smaller than the deviation for the mass-like regulator. This observation strongly suggests that the mass-like regulator should be discarded for quantitative considerations, although it remains, in the present example, a useful regulator for studying the main



qualitative features of the problem.<sup>18</sup> Discarding the mass-like regulator from our discussion, we end up with the observation that the error induced through the scheme dependence is of the same order of magnitude for algebraic as for exponential regulators. For the present case, and at this level of accuracy, no further qualitative differences are observed between the exponential regulators (6.4) and the power-like ones (6.3) for  $n \geq 2$ .

In summary, we conclude that a quantitative analysis of the scheme dependence indeed yields non-trivial information regarding the accuracy of the approximations or truncations employed, as suggested by the qualitative argument presented in Sect. VI A. In addition, we have found some evidence for why a mass-like regulator, as opposed to exponential or higher order power-like regulators, should be discarded for accurate quantitative considerations. However, as the qualitative features are still well described by a mass-like regulator, and as the quantitative deviation is not too big, this also suggests that a mass term regulator could be very useful for an error estimate.<sup>19</sup> Typically, analytical computations are largely simplified for mass-like regulators, allowing for a simple cross-check of the results.

## VII. SUMMARY AND OUTLOOK

We have studied in detail the first-order phase transition of Abelian Higgs models in 3+1 dimensions at finite temperature. Properties of the transition are determined by the underlying fixed point structure of the  $3d$  theory such as the cross-over of the Abelian charge from the Gaussian to the Abelian fixed point. We computed all physical observables at the phase transition, the phase diagram in the domain of first-order transitions and the tri-critical point. The analysis has been restricted to the region of parameter space where the dimensional reduction scenario applies and a perturbative matching of the  $4d$  parameters to the corresponding  $3d$  ones is possible. The main contribution to the free energy (and thus to the physical observables at criticality) stem from the remaining effective  $3d$  running for which we have used a Wilsonian renormalisation group to leading order in the derivative expansion, neglecting the scalar, but not the gauge field anomalous dimension. The latter is related to the non-trivial running of the Abelian gauge coupling, which is described by an effective fixed point. While this fixed point is well understood in the large- $N$  limit where the tri-critical fixed point is known, its precise form is not yet established for the relevant case of  $N = 1$ . We therefore studied the parametric dependence of physical observables on the fixed point value. A quantitative discussion of the relevant physical scales, which are easily accessible within a Wilsonian framework, has also been given.

The main effect on physical observables due to the presence of a non-trivial fixed point depends on the ratio between the cross-over scale  $k_{\text{cr}}$  (which defines the cross-over to the Abelian fixed point) and the typical scales characterising the first-order phase transition

---

<sup>18</sup>This conclusion coincides with those of [22] based on more formal considerations regarding mass-like regulators.

<sup>19</sup>An error estimate based on the mass-like regulator is rather conservative as it seems to overestimate the scheme dependence.

(like the discontinuity scale  $k_{\text{dis}}$ , or  $k_{\text{stable}}$ ). For  $k_{\text{cr}}$  small as compared to  $k_{\text{stable}}$  the observed dependence is weak. The sizeable deviations from the perturbative  $\bar{e}^2(k) \approx \bar{e}^2(\Lambda)$ -behaviour only set in at very small scales below  $k_{\text{stable}}$  and are no longer relevant for the phase transition itself in this situation. The main effects are restricted to alterations in the far infra-red region, like the details of the flattening of the inner part of the potential. On the other hand, a strong dependence emerges for  $k_{\text{cr}}$  larger than  $k_{\text{stable}}$ .

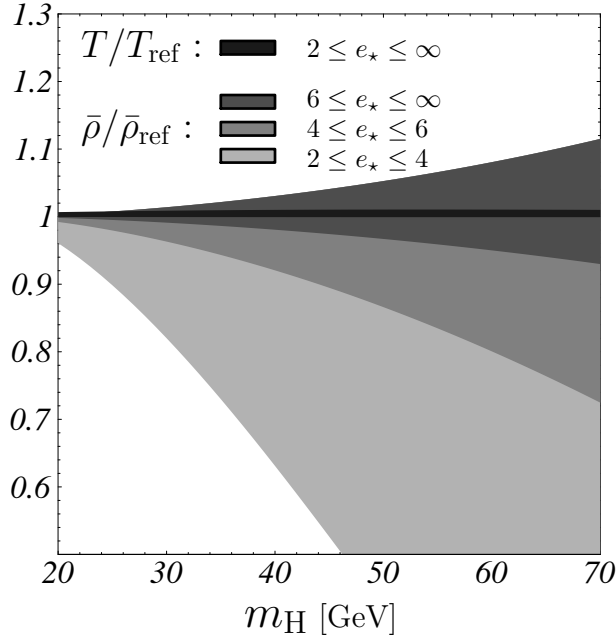


FIG. 15. The relative variation of  $T_c$  and  $\bar{\rho}_0$  with the effective Abelian fixed point. Here, the regions  $T/T_{\text{ref}}$  and  $\bar{\rho}/\bar{\rho}_{\text{ref}}$  compare the critical temperature and the v.e.v. as a function of  $e_*$ . The reference values are obtained for  $e_* = \sqrt{6}\pi \approx 7.7$ .

Most of our results for the physical observables can be summarised as in Fig. 15. Here, the reference values  $T_{\text{ref}}$  and  $\bar{\rho}_{\text{ref}}$  are given for  $e_* = \sqrt{6}\pi$  (which corresponds roughly to  $k_{\text{cr}} \approx k_{\text{stable}}$ ), and for the sharp cut-off regulator. In the present approximation, the critical temperature is insensitive to the running gauge coupling. On the other hand, the v.e.v. appears to be quite sensitive to the actual fixed point value, in particular for larger Higgs field mass. The phase transition weakens significantly for small fixed point values. The reason is that the gauge coupling is decreasing strongly for small fixed point values at scales larger than the scale where the critical potential reaches its degenerate shape, that is above the scale of decoupling. These results compare well with perturbation theory, except for very large or very small values for the Abelian fixed point. Corrections due to the non-trivial scaling of  $\bar{e}^2(k)$  remain below 10% for  $e_*^2 > 6\pi^2$  and  $m_{\text{H}}$  below 70 GeV, but do grow large as soon as  $e_*^2$  is below  $6\pi^2$ . We conclude that  $e_*^2 \approx 6\pi^2$  is a good leading order approximation for small Higgs field mass as higher order corrections are small. For  $m_{\text{H}} = 30$  GeV, we also compared the value for the critical temperature with lattice simulations and found agreement below 4%. The sensitivity on  $e_*^2 < 6\pi^2$  for larger Higgs mass, in turn, requires a better determination of the fixed point in this domain. This concerns in particular physical

observables like the critical exponents at the endpoint of the line of first order phase transitions.

For generic regulator function the free energy in the type-I regime has been given as an integral (one remaining integration). For the case of a sharp cut-off regulator, we obtained an explicit analytical solution for the free energy, given the non-trivial scale dependence of the Abelian charge. In the present article, we evaluated all relevant quantities for initial conditions obtained from a perturbative dimensional reduction scenario relevant for a high temperature (cosmological) phase transition.

The explicit result for the effective potential can also be of use for applications to the superconducting phase transition, or for the nematic to smectic-A phase transition in certain liquid crystals. The main change would concern the initial potential for the effective  $3d$  flow of the potential, and the numerical value of the Abelian charge at that scale. These changes affect in particular the ratio  $k_{\text{cr}}/k_{\text{stable}}$ , and therefore the above discussion, as both scales depend in a qualitatively different manner on  $e^2(\Lambda)$  and  $U_\Lambda$ .

In addition, we studied the dependence of our results on the coarse graining procedure employed. We have seen that the physical observables do depend only very weakly on the coarse graining. This is encouraging, as a strong dependence would have cast serious doubts on the approximations used. Furthermore, we employed a variety of qualitatively different coarse grainings ranging from the mass-like and other polynomial regulators over exponential ones to the sharp cut-off regulator. Therefore, our result can be seen as an important consistency check of the method. The weak variation w.r.t. the coarse graining which is to be interpreted as an ‘error bar’ for the observables, is smaller or of about the same size as the error expected from higher order operators for the coarse grainings studied. This ‘error bar’ would vanish only if no truncation to the effective action would have to be performed. We also observed an intimate relationship between the truncation of the effective action, and the error bar introduced through the scheme dependence. More precisely, it is observed that the scheme dependence is largest in regions where a similarly large effect due to the neglecting of the scalar fluctuations in the non-convex region of the potential is expected. While this result is not entirely unexpected, a quantitative evidence for it has never been presented before. It would be useful if further quantitative results in this direction could be established. This concerns in particular the cross-dependences between an optimal coarse-graining that minimizes the scheme dependence, and an optimized convergence of systematic truncations and approximations [34].

An important open question for future work concerns the precise IR behaviour of the Abelian charge. This, of course, is an intrinsic problem of the  $3d$  theory. As argued, our current understanding is mainly limited due to an insufficient understanding of the field and/or momentum dependence of the Abelian charge. It might be fruitful to consider alternatively a thermal renormalisation group to improve the situation [24]. At the same time, the inclusion of higher order corrections due to scalar fluctuations will also become important – close to the critical points – for a reliable determination of critical exponents and other universal quantities. It would also be interesting to consider the  $SU(2)$ -Higgs theory, where a non-trivial endpoint of the line of first-order phase transitions has been established recently. A field theoretical understanding of this endpoint is still missing, and a derivation of the related critical indices from field theory would be desirable. Again, one expects that the IR

behaviour of the gauge coupling, in competition with the scalar fluctuations, is responsible for the existence of the endpoint.

## APPENDIX A: RS DEPENDENCE AND THRESHOLD FUNCTIONS

The solution of the flow equation (and the related physical observables) can be written as momentum integrals over a measure, which depends on the precise implementation of the coarse graining. We employ the notation of [13], where a scheme dependent measure has been given (in  $d$  dimensions) as

$$I_r[f] = -\frac{d}{2} \int_0^\infty dy \frac{r'(y)}{(1+r(y))^{1+d/2}} f(y) \quad (\text{A.1})$$

for momentum-dependent functions  $f(y)$ , where  $y = q^2/k^2$ , and  $q$  is the loop momenta. As a consequence of the conditions (6.1) on the regularisation function  $r(y)$  it follows that the momentum measure  $-r'(y)/(1+r)^{1+d/2}$  is peaked. The measure is normalised to one,

$$I_r[1] = 1. \quad (\text{A.2})$$

This implies that  $I_r[f]$  depends on the coarse graining as soon as  $f$  displays a non-trivial dependence on momenta.

As an example, let's consider the threshold functions  $\ell_n^d(\omega)$ , defined as

$$\ell_n^d(\omega) = -(\delta_{n,0} + n) \int_0^\infty dy \frac{r'(y)y^{1+d/2}}{[y(1+r) + \omega]^{n+1}}. \quad (\text{A.3})$$

They are related to the above measure through

$$\ell_n^d(\omega) = \frac{2}{d} (\delta_{n,0} + n) I_r \left[ \frac{P^{d+2}}{(P^2 + \omega)^{n+1}} \right]. \quad (\text{A.4})$$

Here, we also introduced the dimensionless effective (regularised) inverse propagator

$$P^2(y) = y + y r(y). \quad (\text{A.5})$$

The threshold functions can always be expanded as a Taylor series in powers of  $\omega$ . Let us define the corresponding RS dependent expansion coefficients

$$a_k = I_r[P^{-k}], \quad (\text{A.6})$$

which are the  $k^{\text{th}}$  moments of  $1/P$  w.r.t. the measure  $I_r$ . These coefficients appear in the computation of the endpoint of the critical line (6.6), which is proportional to the coefficient  $a_1$ . For a power-like regulator  $r(y) = y^{-n}$  [see eq. (6.3)] we find for arbitrary dimension  $d$

$$a_k = \frac{d}{2} \Gamma\left[1 + \frac{k}{2n}\right] \frac{\Gamma\left[\frac{d}{2} + \frac{k}{2}\left(1 - \frac{1}{n}\right)\right]}{\Gamma\left[1 + \frac{d}{2} + \frac{k}{2}\right]}. \quad (\text{A.7})$$

A more detailed discussion of these coefficients and a related discussion of the convergence of amplitude expansions and optimised coarse-graining parameters is given in [34].

## APPENDIX B: THE FLUCTUATION INTEGRAL

The fluctuation integral reads

$$\Delta_k(\bar{\rho}) = -\frac{1}{2\pi^2} \int_k^\Lambda d\bar{k} \int_0^\infty dy \frac{\bar{k}^2}{P^2} \frac{2e_*^2 \bar{\rho} r'(y) y^{5/2}}{2e_*^2 \bar{\rho} + P^2 \bar{k}(1 + \bar{k}/k_{\text{cr}})} \quad (\text{B.1})$$

Note that we have normalised  $\Delta(0) = 0$  in the above definition. The remaining integrals in (B.1) can be solved in different ways, either first performing the momentum integration or the scale integration. Integrating first w.r.t.  $\bar{k}$  yields (for the notation see Appendix A)

$$\Delta_k(\bar{\rho}) = I_r [\mathcal{U}(\bar{\rho}, P)] \quad (\text{B.2})$$

where

$$\begin{aligned} 3\pi^2 \mathcal{U}(\bar{\rho}, P) &= 2e_*^2 \bar{\rho} \int_k^\Lambda d\bar{k} \frac{P^3 \bar{k}^2}{P^2 \bar{k}(1 + \bar{k}/k_{\text{cr}}) + 2e_*^2 \bar{\rho}} \\ &= -2e_*^2 \bar{\rho} P k_{\text{cr}}(k - \Lambda) + e_*^2 \bar{\rho} P k_{\text{cr}}^2 \ln \left( \frac{2e_*^2 \bar{\rho}/P^2 + k + k^2/k_{\text{cr}}}{2e_*^2 \bar{\rho}/P^2 + \Lambda + \Lambda^2/k_{\text{cr}}} \right) \\ &\quad + 2e_*^2 \bar{\rho} P k_{\text{cr}}(4e_*^2 \bar{\rho}/P^2 - k_{\text{cr}}) G_{k,\Lambda}(1 - 8e_*^2 \bar{\rho}/P^2 k_{\text{cr}}) , \end{aligned} \quad (\text{B.3})$$

with  $I_r$  defined in (A.1) and  $P(y)$  in (A.5). The function  $G(\Omega)$  reads

$$G_{k,\Lambda}(\Omega) = \begin{cases} \frac{1}{2\sqrt{\Omega}} \ln \left( \frac{1 + 2k/k_{\text{cr}} - \sqrt{\Omega}}{1 + 2k/k_{\text{cr}} + \sqrt{\Omega}} \frac{1 + 2\Lambda/k_{\text{cr}} + \sqrt{\Omega}}{1 + 2\Lambda/k_{\text{cr}} - \sqrt{\Omega}} \right) & \text{for } \Omega > 0 \\ \frac{-1}{\sqrt{-\Omega}} \left[ \arctan \left( \frac{\sqrt{-\Omega}}{1 + 2k/k_{\text{cr}}} \right) - \arctan \left( \frac{\sqrt{-\Omega}}{1 + 2\Lambda/k_{\text{cr}}} \right) \right] & \text{for } \Omega < 0 \\ \frac{2k_{\text{cr}}(k - \Lambda)}{(k_{\text{cr}} + 2k)(k_{\text{cr}} + 2\Lambda)} & \text{for } \Omega = 0 . \end{cases} \quad (\text{B.4})$$

For a sharp cut-off regulator (6.5), the remaining momentum integration can be performed analytically to give

$$\begin{aligned} 2\pi^2 \Delta_k^{(s)} &= \frac{1}{3} \Lambda^3 \ln \left( 1 + \frac{2e_*^2 \bar{\rho} k_{\text{cr}}}{\Lambda(\Lambda + k_{\text{cr}})} \right) - \frac{1}{3} k^3 \ln \left( 1 + \frac{2e_*^2 \bar{\rho} k_{\text{cr}}}{k(k + k_{\text{cr}})} \right) - \frac{1}{3} k_{\text{cr}}^3 \ln \left( \frac{\Lambda + k_{\text{cr}}}{k + k_{\text{cr}}} \right) \\ &\quad + \frac{1}{6} (k_{\text{cr}}^3 - 6e_*^2 \bar{\rho} k_{\text{cr}}^2) \ln \left( \frac{\Lambda(\Lambda + k_{\text{cr}}) + 2e_*^2 \bar{\rho} k_{\text{cr}}}{k(k + k_{\text{cr}}) + 2e_*^2 \bar{\rho} k_{\text{cr}}} \right) + \frac{4}{3} e_*^2 \bar{\rho} k_{\text{cr}} (\Lambda - k) \\ &\quad - \frac{1}{3} k_{\text{cr}} (-16e_*^4 \bar{\rho}^2 + 10e_*^2 \bar{\rho} k_{\text{cr}} - k_{\text{cr}}^2) G_{k,\Lambda} \left( 1 - 8e_*^2 \bar{\rho}/k_{\text{cr}} \right) . \end{aligned} \quad (\text{B.5})$$

We have normalised  $\Delta(\bar{\rho})$  such that  $\Delta(0) = 0$ .

On the other hand, performing first the scheme dependent momentum integration leaves us with the following remaining integrals,

$$\Delta^{(s)}(\bar{\rho}) = \frac{1}{2\pi^2} \int_k^\Lambda d\bar{k} \bar{k}^2 \ln \left( 1 + \frac{2e_*^2 \bar{\rho}}{\bar{k}(1 + \bar{k}/k_{\text{cr}})} \right) \quad (\text{B.6})$$

$$\Delta^{(m)}(\bar{\rho}) = \frac{1}{2\pi} \int_k^\Lambda d\bar{k} \bar{k}^2 \left( \sqrt{1 + \frac{2e_*^2 \bar{\rho}}{\bar{k}(1 + \bar{k}/k_{\text{cr}})}} - 1 \right) \quad (\text{B.7})$$

$$\Delta^{(q)}(\bar{\rho}) = \frac{1}{\sqrt{2\pi}} \int_k^\Lambda d\bar{k} \bar{k}^2 \left( 1 - \left( 1 + \frac{e_*^2 \bar{\rho}}{\bar{k}(1 + \bar{k}/k_{\text{cr}})} \right)^{-1/2} \right) \quad (\text{B.8})$$

Here, the indices refer to the sharp ( $s$ ), the mass-like ( $m$ ) and the quartic ( $q$ ) cut-off function, as defined in Sect. VI.

### APPENDIX C: INCLUDING SCALAR FLUCTUATIONS

In order to obtain an estimate of the effect of the scalar fluctuations we will solve eq. (2.9) with  $U_k$  on the r.h.s. replaced by  $U_\Lambda$ , for a sharp cut-off regulator. The flow equation becomes

$$4\pi^2 \frac{dU_k(\bar{\rho})}{k^2 dk} = \ell_0^3 \left( \frac{m_{1,\Lambda}^2(\bar{\rho})}{k^2} \right) + \ell_0^3 \left( \frac{m_{2,\Lambda}^2(\bar{\rho})}{k^2} \right) + 2\ell_0^3 \left( \frac{2\bar{e}_3^2(k)\bar{\rho}}{k^2} \right). \quad (\text{C.1})$$

with the masses  $m_i^2$  given through

$$m_1^2(\bar{\rho}) = m_{\text{R}}^2 + \bar{\lambda}_{\text{R}}\bar{\rho}, \quad m_2^2(\bar{\rho}) = m_{\text{R}}^2 + 3\bar{\lambda}_{\text{R}}\bar{\rho}. \quad (\text{C.2})$$

We introduce the functions

$$\begin{aligned} K(m^2) &= -\frac{1}{4\pi^2} \int_\Lambda^k dy y^2 \ln \left( 1 + \frac{m^2}{y^2} \right) \\ &= -\frac{1}{12\pi^2} \left[ 2m^2 k - 2m^3 \arctan \left( \frac{k}{m} \right) + k^3 \ln \left( 1 + \frac{m^2}{k^2} \right) - (k \leftrightarrow \Lambda) \right] \end{aligned} \quad (\text{C.3})$$

$$J_i(\bar{\rho}) = K[m_i^2(\bar{\rho})] - K[m_i^2(0)]. \quad (\text{C.4})$$

The solution to the flow (C.1) then obtains, using also  $\Delta^{(s)}$  from (B.5), as

$$U_k(\bar{\rho}) = U_\Lambda(\bar{\rho}) + \Delta^{(s)}(\bar{\rho}) + J_1(\bar{\rho}) + J_2(\bar{\rho}). \quad (\text{C.5})$$

The effect of the additional terms on the shape of the critical potential is about a few percent, increasing towards higher values for  $m_{\text{H}}$ .

- [1] B.I. Halperin, T.C. Lubensky and S. Ma, Phys. Rev. Lett. **32** (1974) 292;  
H. Kleinert, *Gauge fields in condensed matter* (World Scientific, 1989).
- [2] P.G. de Gennes and J. Prost, *The Physics of Liquid Crystals* (Cambridge Univ. Press, 1993).
- [3] F.J. Wegner and A. Houghton, Phys. Rev. **A8** (1973) 401;  
K.G. Wilson and I.G. Kogut, Phys. Rep. **12** (1974) 75.

- [4] J. Polchinski, Nucl. Phys. **B231** (1984) 269.
- [5] C. Wetterich, Nucl. Phys. **B352** (1991) 529;  
Phys. Lett. **B301** (1993) 90; Z.Phys. **C57** (1993) 451.
- [6] M. Reuter and C. Wetterich, Nucl. Phys. **B391** (1993) 147; **B408** (1993) 91; **B427** (1994) 291.
- [7] D. O'Connor, C.R. Stephens and F. Freire, Mod. Phys. Lett. **A8** (1993) 1779.
- [8] N. Tetradis and C. Wetterich, Nucl. Phys. **B398** (1993) 659.
- [9] B. Bergerhoff, F. Freire, D.F. Litim, S. Lola and C. Wetterich, Phys. Rev. **B53** (1996) 5734,  
[hep-ph/9503334].
- [10] B. Bergerhoff, D.F. Litim, S. Lola and C. Wetterich, Int. J. Mod. Phys. **A11** (1996) 4273,  
[cond-mat/9502039].
- [11] N. Tetradis and D.F. Litim, Nucl. Phys. **B464** (1996) 492, [hep-th/9512073].
- [12] N. Tetradis, Nucl. Phys. **B488** (1997) 92, [hep-ph/9608272].
- [13] D.F. Litim, Phys. Lett. **B393** (1997) 103, [hep-th/9609040].
- [14] W. Buchmüller, T. Helbig and D. Waliser, Nucl. Phys. **B407** (1993) 387.
- [15] A. Hebecker, Z. Phys. **C60** (1993) 271, [hep-ph/9307268].
- [16] W. Buchmüller, Z. Fodor and A. Hebecker, Nucl. Phys. **B447** (1995) 317, [hep-ph/9502321].
- [17] P. Dimopoulos, K. Farakos and G. Koutsoumbas, Eur. Phys. J. C **1** (1998) 711 [hep-lat/9703004].
- [18] K. Kajantie, M. Karjalainen, M. Laine and J. Peisa, Phys. Rev. **B57** (1998) 3011,  
[cond-mat/9704056]; Nucl. Phys. **B520** (1998) 345, [hep-lat/9711048].
- [19] U. Ellwanger, Phys. Lett. **B335** (1994) 364, [hep-th/9402077].
- [20] F. Freire and C. Wetterich, Phys. Lett. **B380** (1996) 337, [hep-th/9601081].
- [21] D.F. Litim and J.M. Pawłowski, Phys. Lett. **B435** (1998) 181, [hep-th/9802064];  
Nucl. Phys. **B74** (PS) (1999) 329, [hep-th/9809023]; **B74** (PS) (1999) 325, [hep-th/9809020].
- [22] D.F. Litim and J.M. Pawłowski, *On gauge invariant Wilsonian flows*, [hep-th/9901063].
- [23] T. Morris, Phys. Lett. **B329** (1994) 241, [hep-ph/9403340].
- [24] D.F. Litim, *Wilsonian flow equations and thermal field theory*, [hep-ph/9811272].
- [25] M. d'Attanasio and M. Pietroni, Nucl. Phys. **B498** (1997) 443, [hep-th/9611038].
- [26] K. Kajantie, M. Laine, K. Rummukainen and M. Shaposhnikov, Nucl. Phys. **B458** (1996) 90,  
[hep-ph/9508379].
- [27] D.F. Litim, C. Wetterich and N. Tetradis, Mod. Phys. Lett. **A12** (1997) 2287, [hep-ph/9407267].
- [28] S. Coleman and E. Weinberg, Phys. Rev. **D7** (1973) 1888.
- [29] N. Tetradis and C. Wetterich, Nucl. Phys. **B383** (1992) 197.
- [30] K. Farakos, K. Kajantie, K. Rummukainen and M. Shaposhnikov, Nucl. Phys. **B425** (1994) 67,  
[hep-ph/9404201].
- [31] A. Strumia and N. Tetradis, Nucl. Phys. **B554** (1999) 697, [hep-ph/9904246].
- [32] P. Arnold and L. Yaffe, Phys. Rev. **D49** (1994) 3003, [hep-ph/9312221].
- [33] P. Arnold and D. Wright, Phys. Rev. **D55** (1997) 6274, [hep-ph/9610226].
- [34] D.F. Litim, Phys. Lett. **B486** (2000) 92, [hep-th/0005245]; hep-th/0103195.